

Non-orthogonal Theory of Polarons and Application to Pyramidal Quantum Dots

D. Obreschkow^{1,3}, F. Michelini^{2,3}, S. Dalessi³, E. Kapon³, and M.-A. Dupertuis³

¹ Physics Department, Oxford University, Oxford OX1 3PU, United Kingdom

² Provence Material and Microelectronics Laboratory (L2MP), 13384 Marseille Cedex 13, France

³ École Polytechnique Fédérale de Lausanne (EPFL),

Laboratory of Physics of Nanostructures, CH-1015 Lausanne, Switzerland

(Dated: February 25, 2019)

A general theory for semiconductor polarons is presented in the framework of the Fröhlich interaction. The theory addresses the electron-phonon interaction by the direct and consistent use of *non-orthogonal* phonon creation operators, which naturally span the set of unique crystal vibrations that couple the confined electronic states of the structure. This setting proves powerful for effective mathematical simplification and convergence, as well as physical interpretation. The theory is particularly well adapted for strong electron-phonon coupling, such as found in quantum dot (QD) structures. In the latter case we explicitly analyze the zero and one-phonon coupling: the qualitative structure of the energy spectrum and the geometry of QD polarons can be easily predicted using a novel non-orthogonal polaron basis, herein baptized "the natural basis". Electronic degeneracies are studied in detail and are shown to generate unentangled zero-shift polarons, which are rigorously eliminated in the natural basis. These developments are applied to realistic pyramidal GaAs QDs. The energy spectrum and the 3D-geometry of polarons are computed and analyzed, and prove that realistic pyramidal QDs clearly fall in the regime of strong coupling. Further investigation reveals an unexpected substructure of "weakly coupled strong coupling regimes", a novel concept originating from overlap considerations. Using Bennett's entanglement measure, we finally present a useful alternative characterization of the strong electron-phonon coupling in QDs.

I. INTRODUCTION

Quantum structures (QSs), such as quantum dots (QDs), are the ultimate solid-state pieces for exciting fundamental researches as well as novel applications in quantum optics and quantum informatics. Today, QDs find technological use in QD lasers,¹ infrared photodetectors,² single photon sources^{3,4} or markers in biology.⁵ Cutting-edge research features QDs as medical fluorophores for *in vivo* detection of cell structures such as tumors.⁶ Other promising applications for QDs are solar cells⁷ and optical telecommunication.⁸ The most exciting, yet challenging expectation relies in the use of QDs as qubit holders and gates for quantum computation.⁹ For fundamental science QDs are among the few systems allowing controlled experiments with single energy quanta giving direct access to controlled quantum entanglement and correlations.

Due to their extreme carrier sensitivity, much interest in QDs relates to carrier relaxation and excitation processes mediated by various interactions, such as carrier-carrier, carrier-photon and carrier-phonon interactions. As for carrier-phonon interactions, early perturbative approaches with acoustic phonons resulted in the *bottleneck concept*.^{10,11,12,13} These perturbative results predict inefficient carrier relaxation for a large class of small QDs, but failed later experimental verification.^{14,15} A definite progress was made with non-perturbative investigations of the deformation potential and Fröhlich interaction, revealing the existence of a strong coupling regime, which is out of reach of perturbative approaches and allows efficient carrier relaxation through acoustic and optical phonon dynamics respectively.^{16,17,18,19} This fact led to the new concept of quantum dot polarons (QDPs), which are non-separable fundamental excitations determined by

the carrier-phonon interaction. Within the approximation of monochromatic LO-modes for the Fröhlich interaction, further simplifications occur. In particular electrons only couple to a finite number of lattice modes as analytically explained through an orthogonal Hilbert space decomposition introduced by Stauber *et al.*²⁰ Their procedure constructs an orthonormalized basis of relevant lattice modes from the finite set of phonon creation/annihilation operators naturally appearing in the Fröhlich Hamiltonian. This leads to a numerically solvable model of QDPs²¹, which can be viewed as an extension of the work of Ferreira *et al.*²²

In this work, the polaron problem is tackled from a different viewpoint: the *full* electron-phonon Hamiltonian is reformulated in terms of the natural *non-orthogonal* phonon creation/annihilation operators of the interaction part. Without requiring additional mathematical complexity, the non-orthogonal structure is kept from the beginning to the end. That powerful theoretical setting exhibits undisputable advantages for computation and physical understanding that fully reveal themselves in the QDP problem. General analytical results applicable to any type of semiconductor quantum structure (QS) are derived in the framework of the non-orthogonal polaron theory. They are subsequently applied to peculiar pyramidal C_{3v} GaAs QDs, but the same theoretical scheme could be applied to any other semiconductor QD structure, e.g. zincblende $InAs$ QDs with C_{2v} symmetry²³ or Wurzite GaN QDs with high C_{3v} or C_{6v} symmetry.²⁴

Section II and related appendices (VII A, VII B) present the non-orthogonal theory, developed to separate relevant and non-relevant carrier-phonon states in the polaron problem. The section goes through two successive Hilbert space decouplings based on lattice mode monochromaticity (II B), and coupling substructure for

any finite phonon number (II C). For the latter we discover an important non-trivial requirement when truncating the Hilbert space to a finite phonon number. In section III, the crucial case of QDPs is treated by using a simple one-phonon model. We will provide an explicit non-orthogonal *polaron* basis, baptized the "natural basis" (III A). This basis provides a detailed interpretation of low-energy QD spectra including further reduction due to electronic degeneracies (III B) and group theoretical simplifications (III C). The theory part concludes with some key ingredients for the three-dimensional (3D) numerical code (III D), which namely comprises an adaptive irregular space discretization for computing the Fröhlich matrix elements.

The non-orthogonal theory was successfully applied to realistic pyramidal GaAs QDs with C_{3v} symmetry.²⁵ Section IV presents the resulting 3D-geometry and spectrum of the QDPs, throughout using group theory considerations (IV A, IV B, IV E). Explicit comparison with perturbation theory confirms the existence of a strong coupling regime. Surprisingly, we find significant numerical evidence for an *additional* substructure inside the strong coupling regime. This leads to the novel concept of "weakly coupled strong coupling regimes" (IV C), which can be understood in terms of overlap between confined electrons and phonons. Using Bennett's entanglement measure, we further present a useful alternative characterization of the strong electron-phonon coupling in QDs (IV D). In section V, we report on the general polaron properties that could be expected in other QD systems. A short review and summary on the non-orthogonal theory are finally given in section VI.

II. NON-ORTHOGONAL THEORY FOR POLARON STATES

A. Polaron Hamiltonian in Quantum Structures

We consider a polar semiconductor QS, e.g. dots, wires or wells, in which the carrier evolution is reasonably described by Fröhlich interactions with monochromatic LO-modes. In such a model, the Hamiltonian takes the form

$$H = H^0 + H^{int} \quad (1)$$

$$\begin{aligned} H^0 &= \sum_{\mu} \epsilon_{\mu} a_{\mu}^{\dagger} a_{\mu} \otimes \mathbf{1}_{ph} + \mathbf{1}_e \otimes \epsilon_{LO} \sum_{\mathbf{q}} b_{\mathbf{q}}^{\dagger} b_{\mathbf{q}} \\ H^{int} &= \sum_{\mu\mu'\mathbf{q}} M_{\mu\mu'\mathbf{q}} a_{\mu}^{\dagger} a_{\mu'} \otimes b_{\mathbf{q}} + h.c. \end{aligned}$$

where a_{μ} , a_{μ}^{\dagger} are fermionic annihilation and creation operators of confined conduction electrons [$\mu = (n, \mathbf{k}, \sigma, \dots)$] and $b_{\mathbf{q}}$, $b_{\mathbf{q}}^{\dagger}$ are bosonic annihilation and creation operators of phonons. The scalars ϵ_{μ} are the free electronic energies, $\epsilon_{LO} = \hbar\omega_{LO}$ is the phonon energy assumed constant, and $M_{\mu\mu'\mathbf{q}}$ are the Fröhlich matrix

elements²⁶

$$\begin{aligned} M_{\mu\mu'\mathbf{q}} &= \sqrt{\frac{\hbar\omega_{LO}e^2}{2\epsilon_0 V q^2} \left(\frac{1}{\epsilon_{\infty}} - \frac{1}{\epsilon_{stat}} \right)} \\ &\times \int_{\mathbb{R}^3} d^3x e^{i\mathbf{q}\cdot\mathbf{x}} \psi_{\mu}^*(\mathbf{x}) \psi_{\mu'}(\mathbf{x}) \end{aligned} \quad (2)$$

where ϵ_{stat} and ϵ_{∞} are the static and high frequency dielectric constants, and $\psi_{\mu}(\mathbf{x})$ are the (one-particle) electronic wave functions. Spin indices have been omitted since to a good approximation the system is decoupled and symmetrical in spin degrees of freedom.

The matrix elements (2) can be considered as discrete 3-dimensional functions of \mathbf{q} . They obey relations of linear dependence, as can be seen by choosing the electronic wave functions $\psi_{\mu}(x)$ real (always possible), in which case $M_{\mu\mu'\mathbf{q}} = M_{\mu'\mu\mathbf{q}}$. If there are N orthogonal electron states μ , the number of such relations is $N(N-1)/2$ and the remaining number of linear independent matrix elements writes $N^2 - N(N-1)/2 = N(N+1)/2$.

B. Subspace of relevant lattice modes

We present the exact transformation of the original Hamiltonian including for the first time the uncoupled phonons consistently.

The Fröhlich Hamiltonian is first reformulated as

$$\begin{aligned} H^{int} &= \sum_{\mu\mu'} J_{\mu\mu'} a_{\mu}^{\dagger} a_{\mu'} \otimes B_{\mu\mu'} + h.c. \\ B_{\mu\mu'} &\equiv \frac{1}{J_{\mu\mu'}} \sum_{\mathbf{q}} M_{\mu\mu'\mathbf{q}} b_{\mathbf{q}} \equiv \sum_{\mathbf{q}} L_{\mu\mu'\mathbf{q}} b_{\mathbf{q}} \end{aligned} \quad (3)$$

where $|J_{\mu\mu'}|^2 = \sum_{\mathbf{q}} |M_{\mu\mu'\mathbf{q}}|^2$ quantizes the electron-phonon coupling strength, with $J_{\mu\mu'}$ chosen as a positive real. Equation (3) underscores that only the subspace of lattice modes generated by the operators $B_{\mu\mu'}^{\dagger}$ is involved in the electron-phonon interactions.

The operators $B_{\mu\mu'}^{\dagger}$ are creation operators of interacting phonons, herein called "QS phonons". These N^2 operators obey the same relations of linear dependence as the Fröhlich matrix elements, i.e. $B_{\mu\mu'}^{\dagger} = B_{\mu'\mu}^{\dagger}$ (for real wave functions). The remaining $N(N+1)/2$ independent dimensions²⁰ shall be scanned by a unique pair index $\lambda \equiv \{\mu, \mu'\} \equiv \{\mu', \mu\}$, such that $\{B_{\lambda}^{\dagger}\}$ is a set of linear independent (yet non-orthogonal) creation operators of QS phonons. To express the free evolution H^0 in terms of the new operators $\{B_{\lambda}^{\dagger}, B_{\lambda}\}$, it is necessary to complete them by a set of operators $\{B_{\mathbf{q}}^{\dagger}, B_{\mathbf{q}}\}$ generating the orthogonal complement of the QS phonons. A natural, yet overcomplete choice writes

$$B_{\mathbf{q}}^{\dagger} \equiv (\mathbf{1} - \mathcal{P}) b_{\mathbf{q}}^{\dagger} \quad (4)$$

where \mathcal{P} is the orthogonal projector on the subspace generated by $\{B_{\lambda}^{\dagger}\}$. Thus $(\mathbf{1} - \mathcal{P})$ projects on the orthogonal complement of all QS phonon modes, and $B_{\mathbf{q}}^{\dagger}$ are the creation operators of "uncoupled phonons" associated with

a wave vector \mathbf{q} . The explicit form of $B_{\mathbf{q}}^{\dagger}$ is given in appendix VII A. Such well-defined objects will prove crucial when studying other problems like polaron decay via phonon-phonon interactions.

The above transformation is summarized in a non-orthogonal, reversible mapping,

$$\{b_{\mathbf{q}}^{\dagger}\} \longleftrightarrow \{B_{\lambda}^{\dagger}, B_{\mathbf{q}}^{\dagger}\} \quad (5)$$

The inversion is not unique, therefore it can be performed in various ways. Explicit transformation laws are derived in Appendix VII A, as well as the relations of linear dependence (60) between the operators $B_{\mathbf{q}}^{\dagger}$. In VII A the reader will further find all fundamental commutators like

$$[B_{\lambda}, B_{\mathbf{q}}^{\dagger}] = 0 \quad (6)$$

expressing the orthogonality between QS phonons and uncoupled phonons.

Using (5), the phonon number operator transforms as (see Appendix VII A)

$$\sum_{\mathbf{q}} b_{\mathbf{q}}^{\dagger} b_{\mathbf{q}} = \sum_{\lambda \lambda'} (\Lambda)_{\lambda \lambda'}^{-1} B_{\lambda}^{\dagger} B_{\lambda'} + \sum_{\mathbf{q}} B_{\mathbf{q}}^{\dagger} B_{\mathbf{q}} \quad (7)$$

$$\text{where } \Lambda_{\lambda \lambda'} \equiv [B_{\lambda}, B_{\lambda'}^{\dagger}] = \sum_{\mathbf{q}} L_{\lambda' \mathbf{q}}^* L_{\lambda \mathbf{q}}$$

and the full Hamiltonian (1) becomes

$$H = H^{QSP} + H^{PP} \quad (8)$$

$$H^{QSP} \equiv \sum_{\mu} \epsilon_{\mu} a_{\mu}^{\dagger} a_{\mu} + \epsilon_{LO} \sum_{\lambda \lambda'} (\Lambda)_{\lambda' \lambda}^{-1} B_{\lambda}^{\dagger} B_{\lambda'} + H^{int}$$

$$H^{PP} \equiv \epsilon_{LO} \sum_{\mathbf{q}} B_{\mathbf{q}}^{\dagger} B_{\mathbf{q}}$$

(unity operators and tensor products have been omitted, in particular H^{PP} is considered as including the unit operator in electronic space).

The operators H^{QSP} and H^{PP} act in orthogonal and decoupled subspaces of the full Hilbert space \mathcal{H} (c.f. Eq. (6)) and thus define a unique decomposition

$$\mathcal{H} = \mathcal{H}^{QSP} \oplus \mathcal{H}^{PP} \quad (9)$$

such that H^{QSP} has vanishing projection on \mathcal{H}^{PP} and H^{PP} has vanishing projection on \mathcal{H}^{QSP} . The "Hilbert subspace of the quantum structure polarons" \mathcal{H}^{QSP} necessarily contains all eigenstates of H subjected to the Fröhlich interaction H^{int} . Such stationary states are most likely entangled in electronic and phononic coordinates and will be referred to as "quantum structure polarons (QSPs)".²² The "Hilbert subspace of pseudo polarons" \mathcal{H}^{PP} annihilates H^{int} , $H^{int} \mathcal{H}^{PP} = 0$. Its eigenstates, infinitely degenerated, are called "pseudo polarons (PPs)"²² and can be neglected in the particular problem of finding the stationary polaron states. Hence, the latter reduces dramatically to solving H^{QSP} inside \mathcal{H}^{QSP} .

It is worth noting that the Hamiltonian (8) manifestly conserves the number of electrons and uncoupled phonons. Therefore the approach developed in this section is not only applicable to any QS, but it can be trivially generalized to the exciton-polaron or even polarons associated with bigger electron/hole complexes.

C. Non-trivial Coupling Tree

Using the non-orthogonal phonon operators $\{B_{\lambda}^{\dagger}, B_{\lambda}\}$ we shall now show that the electron-phonon coupling exhibits a non-trivial structure. This implies a novel and non-trivial prescription for treating polarons with finite phonon numbers. We restrict our considerations to polarons with one electron populating a non-degenerate electronic level structure. The more general case of degenerate levels will be discussed in section III B.

Our procedure explores the action of the Hamiltonian H^{QSP} on different eigenstates of the phonon number operator in order to construct a "coupling tree" with different levels corresponding to different numbers of phonons. Since H^{QSP} vanishes inside \mathcal{H}^{PP} (see II B), we shall focus on the subspace \mathcal{H}^{QSP} , which is from here on restricted to states with an electron number equal to one.

The coupling tree construction is efficiently performed using "additive space operators" (ASOs), defined as additive applications \mathcal{L} from a full set of subspaces onto itself, i.e. $\mathcal{L}(\mathcal{H}_s) \subset \mathcal{H}$ and $\mathcal{L}(\mathcal{H}_s \oplus \mathcal{H}_{s'}) = \mathcal{L}\mathcal{H}_s \oplus \mathcal{L}\mathcal{H}_{s'}$, $\forall \mathcal{H}_s, \mathcal{H}_{s'} \subset \mathcal{H}$. By its additivity an ASO is entirely defined by its action on a complete set of one-dimensional subspaces of \mathcal{H} . Our first example is the "free evolution space operator" \mathcal{F} , which acts inside \mathcal{H}^{QSP} and takes each one-dimensional subspace $\text{vect}\{|\varphi\rangle\}$, $|\varphi\rangle \in \mathcal{H}^{QSP}$, to the space spanned by the evolution of $|\varphi\rangle$ under H^0 ,

$$\mathcal{F}(\text{vect}\{|\varphi\rangle\}) \equiv \text{vect}\{e^{iH^0 t} |\varphi\rangle : \forall t\} \quad (10)$$

To visualize this operation, it is helpful to decompose $|\varphi\rangle$ in eigenstates of H^0 ,

$$|\varphi\rangle = \sum_{\mu, k} \mathcal{P}_{\mu, k} |\varphi\rangle \quad (11)$$

where $\mathcal{P}_{\mu, k}$ are the orthogonal projectors on the eigenspaces of H^0 , associated with the electronic label μ and k phonons. Invoking the relation $e^{iH^0 t}(\mathcal{P}_{\mu, k} |\varphi\rangle) = e^{i(\epsilon_{\mu} + k\epsilon_{LO})t/\hbar}(\mathcal{P}_{\mu, k} |\varphi\rangle)$ and substituting (11) in (10) implies

$$\mathcal{F} \text{vect}\{|\varphi\rangle\} = \text{vect}\{\mathcal{P}_{\mu, k} |\varphi\rangle : \forall \mu, k\} \quad (12)$$

In the following, we shall use the short hand notation

$$\mathcal{F} = \bigoplus_{\mu, k} \mathcal{P}_{\mu, k} \quad (13)$$

An elementary Fröhlich interaction followed by a free evolution under H^0 is expressed by the ASO \mathcal{D}

$$\mathcal{D} \equiv \mathcal{F} H^{int} = \bigoplus_{\mu, k} \mathcal{P}_{\mu, k} H^{int} \quad (14)$$

If \mathcal{D} acts on an eigenspace of the phonon number operator, the sum over k disappears and \mathcal{D} can be expressed as

$$\mathcal{D} = \mathcal{D}^+ \oplus \mathcal{D}^- \quad (15)$$

$$\begin{aligned} \mathcal{D}^+ &\equiv \bigoplus_{\mu} \left(\sum_{\mu'} J_{\mu\mu'} a_{\mu}^{\dagger} a_{\mu'} B_{\mu\mu'}^{\dagger} \right) \\ \mathcal{D}^- &\equiv \bigoplus_{\mu} \left(\sum_{\mu'} J_{\mu\mu'} a_{\mu}^{\dagger} a_{\mu'} B_{\mu\mu'} \right) \end{aligned}$$

($J_{\mu\mu'} = J_{\mu'\mu}$, real; $B_{\mu\mu'} = B_{\mu'\mu}$) Since \mathcal{D}^+ and \mathcal{D}^- alter the phonon number by one unit, it is useful to decompose \mathcal{H}^{QSP} in subspaces associated with every number k of phonons,

$$\mathcal{H}^{QSP} = \bigoplus_{k=0}^{\infty} \mathcal{H}_{kph}^{QSP} \quad (16)$$

The subspace \mathcal{H}_{0ph}^{QSP} is identical to the full zero-phonon subspace \mathcal{H}_{0ph} , since no zero-phonon state annihilates H^{int} ,

$$\mathcal{H}_{0ph}^{QSP} = \mathcal{H}_{0ph} \equiv \text{vect} \left\{ |\mu\rangle \otimes |0\rangle : \forall \mu \right\} \quad (17)$$

where $|\mu\rangle$ is the electronic state and $|0\rangle$ represents the phonon vacuum. For $k > 0$, we find

$$\mathcal{H}_{kph}^{QSP} = \text{vect} \left\{ |\mu_0\rangle \otimes B_{\mu_1\mu_1}^{\dagger} \cdots B_{\mu_k\mu_k}^{\dagger} |0\rangle : \forall \mu_i, \mu'_i \right\} \quad (18)$$

To uncover the action of the operators \mathcal{D}^{\pm} , we shall introduce the subspaces $\mathcal{H}_{kph}^{QSP,m}$, which are obtained from \mathcal{H}_{kph}^{QSP} by imposing the m index chain conditions $\mu'_1 = \mu_0, \dots, \mu'_m = \mu_{m-1}$, $m \leq k$. Explicitly,

$$\begin{aligned} \mathcal{H}_{kph}^{QSP,m} &= \text{vect} \left\{ |\mu_0\rangle \otimes B_{\mu_0\mu_1}^{\dagger} B_{\mu_1\mu_2}^{\dagger} \cdots B_{\mu_{m-1}\mu_m}^{\dagger} |0\rangle \right. \\ &\quad \left. B_{\mu_{m+1}\mu_{m+1}}^{\dagger} \cdots B_{\mu_k\mu_k}^{\dagger} |0\rangle \right\} \end{aligned} \quad (19)$$

with the convention $\mathcal{H}_{kph}^{QSP,0} \equiv \mathcal{H}_{kph}^{QSP}$. These definitions readily imply

$$\mathcal{H}_{kph}^{QSP,0} \supseteq \mathcal{H}_{kph}^{QSP,1} \supseteq \dots \supseteq \mathcal{H}_{kph}^{QSP,k} \quad \forall k \quad (20)$$

In Appendix VII B we prove the crucial relations,

$$\mathcal{D}^+ \mathcal{H}_{kph}^{QSP,m} = \mathcal{H}_{k+1ph}^{QSP,m+1} \quad m = 0, \dots, k \quad (21)$$

$$\mathcal{D}^- \mathcal{H}_{kph}^{QSP,m} = \mathcal{H}_{k-1ph}^{QSP} \quad m = 0, 1, 2 \quad (22)$$

These relations are illustrated in Fig. 1. We emphasize that it is not generally possible to obtain the whole subspace $\mathcal{H}_{k+1ph}^{QSP}$ by acting with \mathcal{D}^+ on \mathcal{H}_{kph}^{QSP} . However, from (21) and (22) it is easy to see that this link is achieved by the ASO $\mathcal{D}^- \mathcal{D}^+ \mathcal{D}^+$,

$$\mathcal{D}^- \mathcal{D}^+ \mathcal{D}^+ \mathcal{H}_{kph}^{QSP} = \mathcal{H}_{k+1ph}^{QSP} \quad (23)$$

This discussion reveals that all k -phonon states in \mathcal{H}_{kph}^{QSP} , orthogonal to $\mathcal{H}_{kph}^{QSP,1}$, only couple to $(k-1)$ -phonon states through $(k+1)$ -phonon states. We stress an important implication: if, for physical or computational reasons, the model is truncated to a finite number p of phonons, $1 \leq p < \infty$, then the last subspace \mathcal{H}_{pph}^{QSP} must be restricted to $\mathcal{H}_{pph}^{QSP,1}$. Otherwise *non-physical polarons would appear*, that would seem uncoupled and thus unshifted relative to the free spectrum. Such a precaution was apparently not taken in previous works.²¹ The particular truncation $\mathcal{H}_{pph}^{QSP} \rightarrow \mathcal{H}_{pph}^{QSP,1}$ also represents an analytical and computational simplification. Finally one should note that a restriction to a finite phonon number remains a non-perturbative approach, since it does not limit the order of the Fröhlich interaction H^{int} , but only excludes states with higher free energy.

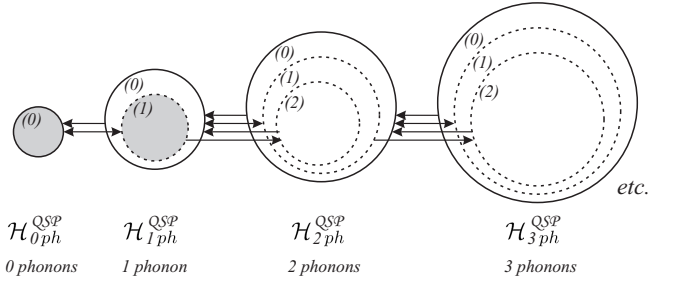


FIG. 1: Coupling structure exhibited by the Fröhlich interaction. Arrows to the right represent the operation \mathcal{D}^+ and arrows to the left represent the operation \mathcal{D}^- . The numbers in brackets (x) indicate the subspaces $\mathcal{H}_{kph}^{QSP,x}$. Gray filling indicates the subspace \mathcal{H}^* spanned by the natural basis (25).

III. ZERO AND ONE PHONON QDPS

In the following, the general quantum structure with which we dealt so far is identified with a quantum dot: $QS \rightarrow QD$. In such zero-dimensional systems, the interactions between bound conduction electrons and lattice displacements are reasonably dominated by Fröhlich interactions of LO-modes. Monochromaticity is also a fairly precise assumption for the relevant modes (*i.e.* long wavelengths with respect to the dot) which proves crucial for the effective reduction of the phonon space: only a finite space of LO lattice modes interacts with dot electron states.^{20,22} The formalism can also be developed in a similar way for holes (although acoustic phonons may have to be taken into account there), or for any many-particle complex such as an exciton-, a trion- or a biexciton-based quantum dot polaron. Stauber and Zimmermann²¹ showed that a correction term must be introduced in the case of non-neutral complexes.

In the next three subsections (III A-III C) we shall investigate a QD model restricted to electronic coupling to at most one phonon, which is a good approximation for the first polaron levels, which are typically populated at low temperatures.

A. Natural Basis

In QD systems, the number of electronic levels in the dot is finite, hence the subspace of relevant lattice modes is finite, too. Those modes are localized about the QD as shown by considering the Fourier transform of the matrix elements $M_{\mu\mu'q}$, appearing in the creation operators $B_{\mu\mu'}^\dagger$. We recall that according to their relations of linear dependence there are only $N(N+1)/2$ relevant dimensions.²⁰ By virtue of the coupling structure developed in the previous paragraph, the one-phonon model is properly represented by the relevant subspace corresponding to gray zones in Fig. 1. It writes

$$\mathcal{H}^* \equiv \mathcal{H}_{0ph}^{QDP} \oplus \mathcal{H}_{1ph}^{QDP,1} = \mathcal{H}_{0ph} \bigoplus_{\mu=1}^N \mathcal{P}_{\mu,1} H^{int} \mathcal{H}_{0ph} \quad (24)$$

Considering \mathcal{H}_{1ph}^{QDP} instead of $\mathcal{H}_{1ph}^{QDP,1}$, would lead to artificial states without electron-phonon coupling. A vector set \mathcal{B}^* , such that $\mathcal{H}^* = \text{vect } \mathcal{B}^*$ is directly obtained from (19). Using the short hand $|\mu; 0\rangle \equiv |\mu\rangle \otimes |0\rangle$ and $|\mu; q\rangle \equiv |\mu\rangle \otimes |q\rangle$, we write

$$\mathcal{B}^* = \left\{ |\mu; 0\rangle, |\mu\rangle \otimes B_{\mu\mu'}^\dagger |0\rangle = \sum_q M_{\mu'\mu q}^* |\mu; q\rangle : \quad \forall \mu, \mu' \right\} \quad (25)$$

Those vectors are generally non-orthogonal but linearly independent and \mathcal{B}^* will be called the "natural basis". All natural basis states are eigenstates of H^0 . For each electronic level μ there is *one* zero-phonon state of energy ϵ_μ and there are N one-phonon states of energy $\epsilon_\mu + \epsilon_{LO}$. Since there are N electronic levels μ , the dimension of the relevant subspace \mathcal{H}^* writes

$$\dim(\mathcal{H}^*) = \text{card}(\mathcal{B}^*) = N(N+1) \quad (26)$$

The requirement to reduce the one-phonon subspace to $\mathcal{H}_{1ph}^{QDP,1}$ reveals the simplifying feature that many product states of electrons and QD phonons are irrelevant for the polaron structure (e.g. $|\mu_1\rangle \otimes B_{\mu_2\mu_3}^\dagger |0\rangle \notin \mathcal{B}^*$). Therefore, the number of QDPs only scales as N^2 and not as N^3 (!), which one might expect from the number N of dot electrons and the number $\propto N^2$ of QD modes.

Fig. 2 shows the qualitative QDP spectrum in the case of a QD with *only three non-degenerate electronic states*. Gray bars denote additional QDPs that would appear in an extended model including the interaction with two-phonon states. Those are associated with free states in \mathcal{H}_{1ph}^{QDP} but orthogonal to $\mathcal{H}_{1ph}^{QDP,1}$. The *connections* between free levels and QDP levels (Fig. 2) are an important outcome of the natural basis. They indicate the free levels from which specific QDPs arise, if one "gradually introduced the Fröhlich interaction". This picture allows a prediction of spectral changes under dot size variation, since one can generally assume that shifts increase when approaching a resonance of the Fröhlich interaction (*i.e.* $\Delta\epsilon = \epsilon_{LO}$).

In conclusion, a complete non-orthogonal polaron basis called the "natural basis" (25) has been introduced. It

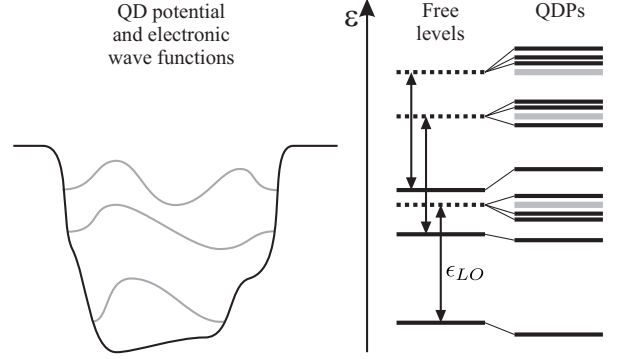


FIG. 2: Qualitative structure of the polaron spectrum in the case of three bound, non-degenerate electronic levels. Each gray bar indicates 3 additional polaron levels that result from interaction with two-phonon states.

provides a mean for physical understanding of polaron spectra involving low phonon numbers, and constitutes a simplifying and powerful computational basis (see III D, IV).

B. Electronic Degeneracies

This section and the next one address electronic degeneracies and point out important features which must be accounted for. In particular, if a non-degenerate electronic spectrum (e.g. Fig. 2) gets partially degenerate, for example by specific dot size adjustment, not only certain QDPs may become degenerate, but some of them will decouple and align with free levels. We shall call such states "zero-shift polarons" and show that they are nothing but uncoupled states, *i.e.* pseudo-polarons susceptible to become QDPs as soon as the degeneracies are lifted. Thus the relevant QDP Hilbert space can be further reduced in case of electronic degeneracies (accidental or symmetry related), such that spurious zero-shift QD polarons are automatically eliminated.

In order to label *accidental* degeneracies, the electron index is now expressed as $\mu \equiv (\tau, i)$, where $\tau = 1 \dots n \leq N$ is an energy index and $i = 1, \dots, g_\tau$ a degeneracy index. The eigenspaces of H^0 are hence indexed by (τ, k) . The respective energies write $\epsilon = \epsilon_\tau + k\epsilon_{LO}$ and the orthogonal projectors on those subspaces are called $\mathcal{P}_{\tau,k}$. Following the method of the operators \mathcal{D}^\pm shown in section II C the relevant subspace writes,

$$\mathcal{H}^* = \mathcal{H}_{0ph} \bigoplus_{\tau=1}^n \mathcal{P}_{\tau,1} H^{int} \mathcal{H}_{0ph} \quad (27)$$

A non-orthogonal natural basis is obtained by expressing \mathcal{H}_{0ph} and $\mathcal{P}_{\tau,1}$ in terms of the basis states $|\mu; 0\rangle$ and $|\mu; q\rangle$,

$$\mathcal{B}^* = \left\{ \left| \tau, i; 0 \right\rangle, \sum_{i'=1}^{g_{\tau'}} \sum_{\mathbf{q}} M_{\tau, i; \tau', i'; \mathbf{q}}^* \left| \tau', i'; \mathbf{q} \right\rangle \right\} \quad (28)$$

Its dimension is

$$\dim(\mathcal{H}^*) = \text{card}(\mathcal{B}^*) = N(n+1) \quad (29)$$

where N is the total number of orthogonal dot electronic states and $n \leq N$ is the number of distinct electronic energies. ($n=N$ is the non-degenerate case.) As in the previous section, the natural basis (28) provides a qualitative prediction of the polaronic spectrum and associates each polaron level with a free level (see example Fig. 3). In particular, we emphasize that the highest free level in the figure only couples with 3 modes and not with 6 as one might expect from pulling together the two uppermost free levels in Fig. 2. The particular case of symmetry related degeneracies is now addressed in the next subsection.

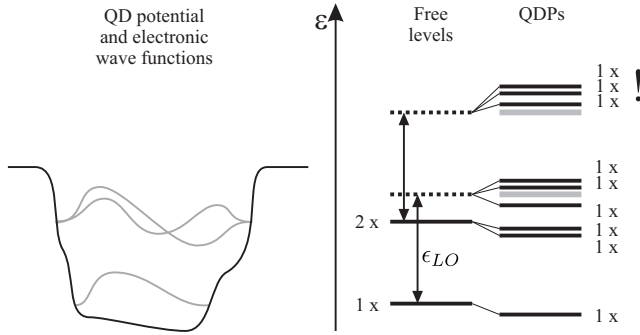


FIG. 3: Qualitative structure of the polaron spectrum in the case of two electronic levels, one of which is twice degenerate. Each gray bar indicates 3 more polarons that result from interaction with two-phonon states.

C. Symmetrical Quantum Dots

Additional degeneracies and simplifications may be obtained in the case of QDs invariant under a set of symmetry operations, generally described by the group of such operations \mathcal{G} , i. e. $[H, g] = 0 \forall g \in \mathcal{G}$. In such a case all stationary states satisfy well defined transformation laws, associated with an irreducible representation (irrep) Γ of dimension d_Γ , which also specifies the respective level degeneracy. For $d_\Gamma > 1$ a degeneracy index $j = 1, \dots, d_\Gamma$, the so-called "partner function", indexes a choice of orthogonal states within the same eigenspace. Expressed for passive transformations the laws read

$$\theta(g)^{-1} \psi_{(\Gamma, j)} = \sum_{i=1}^{d_\Gamma} (D^\Gamma(g))_{ij}^{-1} \psi_{(\Gamma, i)} \quad \forall g \in \mathcal{G} \quad (30)$$

where $D^\Gamma(g)$ is a given set of representation matrices, that characterize the transformation laws of the partner function basis, and can be chosen in a suitable way.

Since all stationary states can be associated with a well defined symmetry (Γ, j) , the Hamiltonian can be pre-diagonalized by finding an orthogonal decomposition of the Hilbert space in subspaces gathering only states with

symmetry (Γ, j). As for the one-phonon/one-electron QD model, this symmetry decomposition writes

$$\mathcal{H}^* = \bigoplus_{\Gamma, j} \mathcal{H}_{\Gamma, j}^* , \quad \mathcal{H}_{\Gamma, j}^* \equiv \mathcal{P}_{\Gamma, j} \mathcal{H}^* \quad (31)$$

where the orthogonal projectors $\mathcal{P}_{\Gamma,j}$ on the subspaces spanned by all the states that satisfy the transformation laws (30) for a given symmetry (Γ, j) can be written as

$$\mathcal{P}_{\Gamma,j} = \frac{d_\Gamma}{|G|} \sum_g \left(D^\Gamma(g)^{-1} \right)_{jj}^* \theta^{-1}(g) \quad (32)$$

The problem of finding the QDPs reduces to solving H^{QDP} inside each relevant subspace $\mathcal{H}_{\Gamma,j}^*$ individually. To provide these subspaces with suitable bases, we require a symmetrized eigenstate basis relative to H^0 , *i.e.* each basis state satisfies the transformation (30) for its particular symmetry (Γ, j) . Such a basis necessarily exists, since H^0 obeys the same symmetry as H , and will be denoted

$$\begin{aligned} \text{electron} : \{|\tau, i\rangle\} &\longleftrightarrow \{|\Gamma_e, j_e, \alpha_e\rangle\} \\ \text{phonon} : \{|\mathbf{0}\rangle, |\mathbf{q}\rangle\} &\longleftrightarrow \{|\mathbf{0}\rangle, |\Gamma_{ph}, j_{ph}, \alpha_{ph}\rangle\} \end{aligned} \quad (33)$$

α_e is usually a sequential index with energy, whereas α_{ph} represents a continuous degeneracy index because of the assumption of LO-phonon monochromaticity. The explicit transformations (33) can be more subtle than anticipated. An example will be developed in detail for the C_{3v} symmetry group in section IV A. These symmetrized bases allow the construction of a symmetrized basis of the tensorial products using *generalized Clebsch-Gordan coefficients* $C_{j_1, l_e, l_{ph}}^{\Gamma_e, \Gamma_{ph}}$ (in the sense of point groups),

$$\begin{aligned}
 (a) \quad & |\Gamma, j; \Gamma_e, \alpha_e; 0\rangle = |\Gamma_e = \Gamma, j_e = j, \alpha_e\rangle \otimes |0\rangle \\
 (b) \quad & |\Gamma, j; \Gamma_e, \alpha_e; \Gamma_{ph}, \alpha_{ph}\rangle \\
 & = \sum_{j_e, j_{ph}} C_{j_e, j_{ph}}^{\Gamma_e, \Gamma_{ph}} |\Gamma_e, j_e, \alpha_e\rangle \otimes |\Gamma_{ph}, j_{ph}, \alpha_{ph}\rangle
 \end{aligned} \tag{34}$$

Here Γ and j refer to the overall symmetry and Γ_e and Γ_{ph} satisfy $\Gamma \subseteq \Gamma_e \otimes \Gamma_{ph}$. The phonon vacuum is always symmetrical, $\Gamma_{ph} = A_1$, and hence the overall representation of a *zero-phonon state* will always be identified with the electron representation, $\Gamma = \Gamma_e$ (EQ. ref{general sym product basis}).

A symmetrized expression of the relevant subspace \mathcal{H}^* immediately results from equation (27) by replacing the electronic energy index τ with the pair index (Γ_e, α_e) . Expressing \mathcal{H}_{0ph} and $\mathcal{P}_{\Gamma_e, \alpha_e, 1ph}$ in terms of the symmetrized product basis (34) directly leads us to a set of non-orthogonal basis vectors, each of which transforms according to (30) for a particular symmetry (Γ, j) . Those vectors can be regrouped in different "natural bases" $\mathcal{B}_{\Gamma, j}^*$ associated with the different subspaces $\mathcal{H}_{\Gamma, j}^*$ defined in (31). The expression of those vectors can be further simplified using the selection rule for the Fröhlich matrix

elements, which results directly from the transformation laws and the invariance of the Hamiltonian,

$$\langle \Gamma, j; \Gamma_e, \alpha_e; \Gamma_{ph}, \alpha_{ph} | H^{int} | \Gamma', j'; \Gamma'_e = \Gamma, \alpha_e; 0 \rangle = 0$$

unless $(\Gamma, j) = (\Gamma', j')$

For the remaining non-vanishing matrix elements, we shall use the notation

$$M_{(\Gamma_e, \alpha_e, \Gamma_{ph}, \alpha_{ph}); \alpha'_e}^{\Gamma, j} \equiv \langle \Gamma, j; \Gamma_e, \alpha_e; \Gamma_{ph}, \alpha_{ph} | H^{int} | \Gamma, j; \Gamma, \alpha'_e; 0 \rangle \quad (35)$$

Finally, the natural bases $\mathcal{B}_{\Gamma,j}^*$ write

$$\mathcal{B}_{\Gamma,j}^* = \left\{ \begin{array}{l} |\Gamma, j; \Gamma, \alpha_e; 0\rangle, \\ \sum_{\Gamma_{ph}, \alpha_{ph}} M_{(\Gamma'_e, \alpha'_e, \Gamma_{ph}, \alpha_{ph}); \alpha_e} \\ \times |\Gamma, j; \Gamma'_e, \alpha'_e; \Gamma_{ph}, \alpha_{ph}\rangle \\ \forall \alpha_e, \Gamma'_e, \alpha'_e \end{array} \right\} \quad (36)$$

The sum goes over all indices, but one assumes that $C = 0$ when Γ_{ph} does not satisfy a selection rule $\Gamma \subseteq \Gamma_e \otimes \Gamma_{ph}$. These bases are mutually orthogonal, but each of them remains non-orthogonal.

The overall symmetry index of an arbitrary natural basis state is always equal to the symmetry index of the involved pure electron state (zero-phonon state), see equations (35,36). Hence, if a certain representation Γ is absent in the considered set of bound electrons, there are *no Γ -like polaron states*, even though we necessarily have Γ -like phonon states (!).

Like in the previous two sections the natural bases (36) provide a prediction of the polaronic spectrum. Fig. 4 shows the particular case of two bound electronic levels, where the second level is twice degenerate by virtue of the underlying dot symmetry. In particular, we emphasize the appearance of degenerate polaron levels, which can be associated with both, a degenerate *or* non-degenerate electron level.

The dimensionality of the different subspaces $\mathcal{H}_{\Gamma,j}^*$ can be directly derived from the number of natural basis states for a given symmetry (Γ, j) and reads

$$\dim(\mathcal{H}_{\Gamma,j}^*) = \text{card}(\mathcal{B}_{\Gamma,j}^*) = n^\Gamma(1+n) \quad (37)$$

where n^Γ is the number of *distinct* electronic energies with a given symmetry Γ ($\alpha_e = 1, \dots, n^\Gamma$), and n denotes the total number of distinct electronic energies ($n = \sum \nolimits^\Gamma n^\Gamma$). The dimension (37) is independent of the partner function j in agreement with the feature that those functions can be defined arbitrarily inside a given representation Γ . Since $\sum_{(\Gamma, j)} \dim(\mathcal{H}_{\Gamma, j}^*)$ equals $\dim(\mathcal{H}^*)$, given in (29), expression (37) is a consistent refinement of the full dimension.

D. Computational Aspects

Finding the polaron spectrum of the one-electron/one-phonon model reduces to diagonalizing the Hamiltonian H^{QDP} inside the low dimensional subspace spanned by

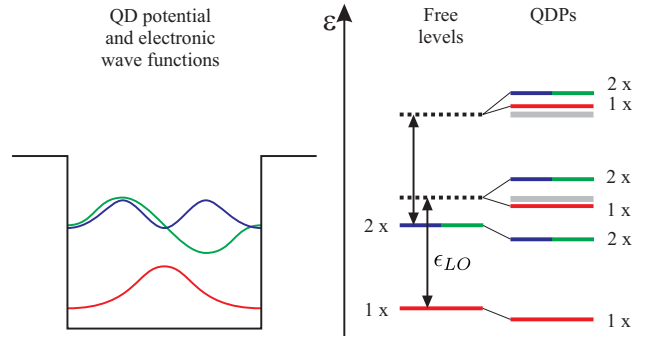


FIG. 4: Qualitative structure of the polaron spectrum in the case of two electronic levels, one of which is twice degenerate due to the dot symmetry. The levels correspond to two different representations Γ marked in red and blue/green. The latter has two dimensions, characterized by the function j . Each gray bar indicates 3 more polarons that result from interaction with two-phonon states.

the natural basis \mathcal{B}^* given in (25), (28) or (36), depending on the physical situation. Although the number of Fröhlich matrix elements for the interaction with LO-phonons has been minimized by the subspace reduction, their prerequisite computation can be numerically intensive for the arbitrary 3D wavefunctions that one should consider in a general case (see section IV where a single wavefunction is typically sampled on 10^6 points). To alleviate this issue we have developed an original *adaptive, irregular* discretization of the reciprocal space for lattice modes, and shown that it was an efficient method, also applicable when working directly with a *non-orthogonal* basis.

The numerical benefit of an irregular reciprocal space discretization relies on the fast variation of the Fröhlich matrix elements in function of the normal mode wave vector \mathbf{q} in certain well localized domains. Increasing the local point density only in those domains remarkably improves the numerical precision with a minor increase of the required computational resources. To generate a well adapted irregular \mathbf{q} -space discretization, we start with a regular coarse mesh covering the first Brillouin zone of the underlying lattice. Thereafter, the various Fröhlich matrix elements are evaluated for all wave vectors \mathbf{q} of the given mesh. This procedure requires a preliminary computation of the volumes associated with each mesh node, taken as the volume of the respective Wigner-Seitz cells (Appendix VII C). The nearest neighbors with the highest difference between their Fröhlich elements are added a new node in between, which provides the initial mesh for the next iteration. This algorithm is repeated until the maximal difference between neighboring Fröhlich matrix elements falls below a preset threshold. Fig. 5 shows the Wigner-Seitz cells generated with this technique in the case of the first Brillouin zone of a body-centered cubic lattice.

After the generation of the irregular \mathbf{q} -space discretization and the computation of the respective Fröhlich matrix elements, the set of natural basis vectors is evaluated.

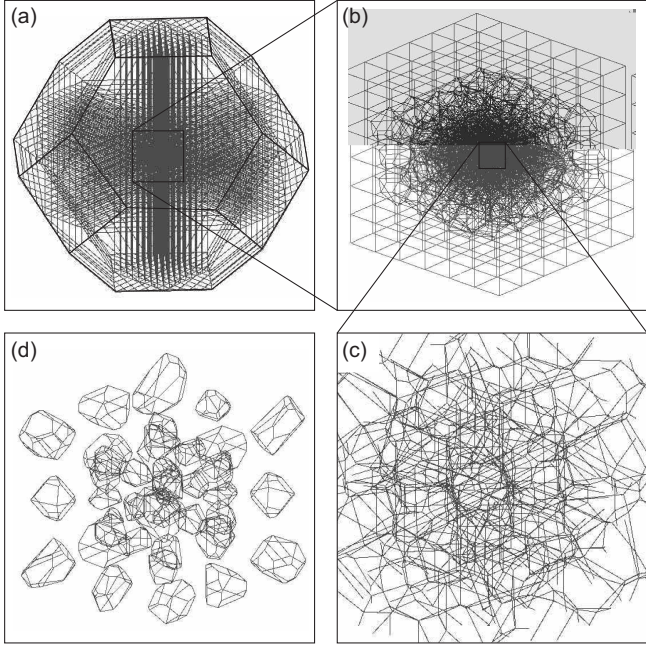


FIG. 5: Polygonal Wigner-Seitz cells of the irregular \mathbf{q} -space discretization. (a)-(c) zoom into first Brillouin zone of a BCC lattice. (d) A few selected Wigner-Seitz cells from a region similar to (c).

allowing to diagonalize the relevant Hamiltonian H^{QDP} .

Let us finally evaluate the numerical value of working with a non-orthogonal basis. The sole consequence is that the standard eigenvalue problem becomes a *generalized eigenvalue problem*, that is an equation of the type

$$\bar{\bar{H}}^{QDP}|\psi\rangle = \epsilon \bar{\bar{S}}|\psi\rangle, \quad (38)$$

$$\bar{\bar{H}}_{\alpha\alpha'}^{QDP} \equiv \langle \alpha | H^{QDP} | \alpha' \rangle, \quad \bar{\bar{S}}_{\alpha\alpha'} \equiv \langle \alpha | \alpha' \rangle \neq \delta_{\alpha,\alpha'}$$

where $|\alpha\rangle$ are the natural basis states, and $\bar{\bar{S}}_{\alpha\alpha'}$ is the so-called "mass matrix". This trade-off is advantageous, since optimized packages for the generalized eigenvalue problem are widely available, and one gets rid of an additional basis change involving a Gram-Schmidt decomposition (often requiring enhanced precision for small scalar products). This is a positive numerical byproduct of the non-orthogonal theory.

With the set of tools presented above, a spectral precision down to 0.01meV for typical QDPs can be reached in characteristic computation times of only *a few minutes* using a standard 3GHz processor. The most computer intensive part is the evaluation of the Fröhlich matrix elements.

IV. APPLICATION TO PYRAMIDAL QDS

A. Symmetrical Model and Non-Orthogonal Basis

We shall now use the general theory of section II to compute the low energy quantum dot polarons (QDPs)

of a realistic pyramidal GaAs/AlGaAs QD.²⁵ This dot is part of a complex heterostructure represented by the geometrical model shown in Fig. 6a.²⁷ We will take full advantage of the underlying C_{3v} -symmetry group, which exhibits only three irreps A_1 , A_2 and E . The latter is two-dimensional and a possible basis results from symmetrizing E -states with respect to the symmetry plane σ_1 (spanned by the [111] and [112] crystalline directions in GaAs/AlGaAs). Thereby the partner function $j = \pm$ is identified with the parity index relative to σ_1 . In graphical representations we shall consistently apply the color scheme: A_1 (red), A_2 (yellow), $E+$ (blue), $E-$ (green). QDPs will be computed using the non-orthogonal natural basis introduced in section III C. This basis will be derived analytically in three stages: (1) individual symmetrization of electronic and phononic eigenstates of H^0 , (2) construction of a symmetrized product basis using Clebsch-Gordon coefficients, and (3) derivation of the symmetrized natural bases for the relevant subspaces $\mathcal{H}_{\Gamma,j}^* \subset \mathcal{H}$.

First, we shall find symmetrized electron and phonon bases. As for the bound electron, all eigenstates of H^0 are automatically symmetrized and hence the task reduces to finding these eigenstates. This was recently achieved by Michelini *et al.*²⁷ For a dot height $h = 10\text{nm}$, there are two A_1 -like levels (non-degenerate) and one E -like level (twice degenerate) as shown in Fig. 6b. In the standard notation of section III C, i. e. $|\Gamma_e j_e, \alpha_e\rangle$, those states write

$$\{|A_1, 1\rangle, |E \pm\rangle, |A_1, 2\rangle\} \text{ electron basis} \quad (39)$$

where the index j_e has been omitted in the case of the one-dimensional A_1 -representations and the index α_e has been omitted for the unique E -level. We note that there are no A_2 -like electron states at low energy, which immediately predicts that there will be *no* A_2 -like QDPs (section III C). For the phonons the symmetrization is inasmuch different as the eigenstates of H^0 , such as plane waves, are *not* automatically symmetrized. This feature relies on the monochromaticity assumption rendering all normal modes degenerate. A symmetrized eigenstate basis is properly derived in Appendix VII D. The resulting basis states superpose six (or four) plane waves, such that the directions of the different wave vectors are mutually related by symmetry operations (see Fig. 6c). We shall label such states with the respective vector \tilde{q} belonging to the subset \mathcal{A} , which constitutes a sixth of the reciprocal space. In the case of E -like superpositions there are two orthogonal states associated with the same vector \tilde{q} . They will be distinguished through the additional index $\xi = 1, 2$ (discussion in Appendix VII D). Finally the phonon basis writes

$$\left\{ |0\rangle, |A_1, \tilde{q}\rangle, |A_2, \tilde{q}\rangle, \right. \left. |E \pm, \tilde{q}, \xi\rangle \right\} \text{ phonon basis} \quad (40)$$

where $|0\rangle$ is the phonon vacuum state (0meV), whilst all other states are one-phonon states (35.9meV).

Second, we construct a symmetrized product basis from (39) and (40) according to Eq.(34). The explicit

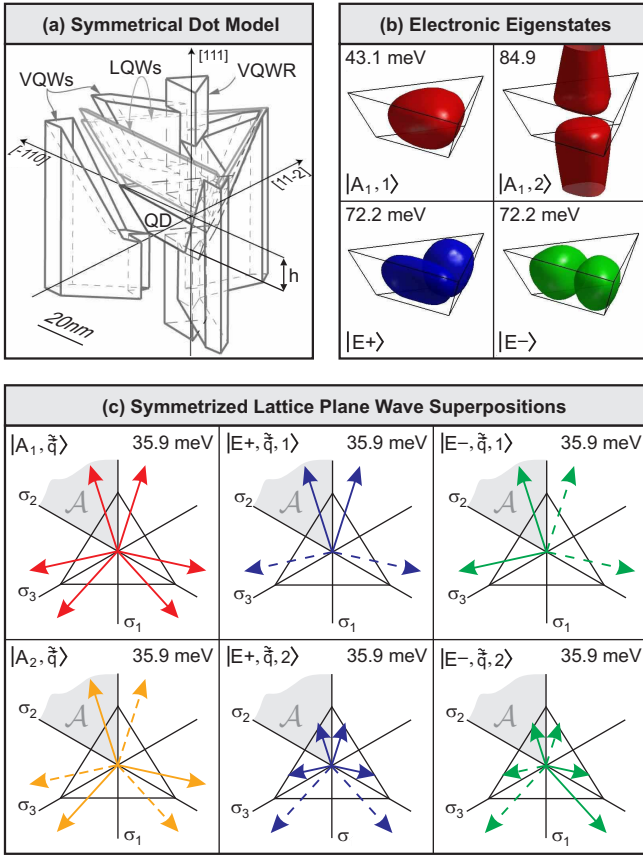


FIG. 6: (a) Numerical model²⁷ of realistic heterostructure with pyramidal QD, vertical quantum wire (VQWR), vertical quantum wells (VQWs) and lateral quantum wells (LQWs). (b) Isosurfaces of envelope functions of the stationary single electron states. (c) Particular plane wave superpositions of symmetrized one-phonon basis. The length of the arrows represents the relative amplitude and dashed arrows have opposite phase.

derivations given in Appendix VII E yield states of the form

$$\left\{ \begin{array}{l} |\Gamma j; \Gamma_e, \alpha_e; 0\rangle, \\ |\Gamma j; \Gamma_e, \alpha_e; \Gamma_{ph}, \tilde{q}, \xi\rangle \end{array} \right\} \text{ product basis} \quad (41)$$

where the first ket represents states with zero phonons and the latter states with one phonon.

Third, we write the natural basis of the relevant Hilbert subspace of \mathcal{H}^* according to the general theory (section III C). This basis decomposes in symmetry-subspaces $\mathcal{H}_{A_1}^*$ (8 dimensions), \mathcal{H}_{E+}^* (4 dimensions), \mathcal{H}_{E-}^* (4 dimensions). Yet, in our particular case the most energetic natural basis states yield energies above the first two-phonon state. To remain consistent with the one-phonon assumption, we shall neglect those states. Thereby the dimensions reduce to 6 ($\mathcal{H}_{A_1}^*$), 3 (\mathcal{H}_{E+}^*) and 3 (\mathcal{H}_{E-}^*). The respective natural bases result from the general expressions (36) and are given in Tab. I and Tab. II.

meV	expressed as symmetrized product states	subspace
43.1	$ A_1; A_1, 1; 0\rangle$	$\mathcal{H}_{A_1, 1}^*$
79.0	$\sum_{\tilde{q}} A_1; A_1, 1; A_1, \tilde{q}\rangle \langle \dots H^{int} A_1; A_1, 1; 0\rangle$	
108.1	$\sum_{\tilde{q}, \xi} A_1; E; E, \tilde{q}, \xi\rangle \langle \dots H^{int} A_1; A_1, 1; 0\rangle$	
84.9	$ A_1; A_1, 2; 0\rangle$	
79.0	$\sum_{\tilde{q}} A_1; A_1, 1; A_1, \tilde{q}\rangle \langle \dots H^{int} A_1; A_1, 2; 0\rangle$	$\mathcal{H}_{A_1, 2}^*$
108.1	$\sum_{\tilde{q}, \xi} A_1; E; E, \tilde{q}, \xi\rangle \langle \dots H^{int} A_1; A_1, 2; 0\rangle$	

TABLE I: Natural basis of the subspace $\mathcal{H}_{A_1}^*$. The bra $\langle \dots |$ is the adjoint of the preceding ket. The two subspaces $\mathcal{H}_{A_1, 1}^*$ and $\mathcal{H}_{A_1, 2}^*$ are defined by the three basis vectors on their left. They constitute so-called "weakly coupled strong coupling subspaces", discussed in section IV C.

meV	expressed as symmetrized product states
72.2	$ E\pm; E; 0\rangle$
79.0	$\sum_{\tilde{q}, \lambda} E\pm; A_1, 1; E, \tilde{q}, \lambda\rangle \langle \dots H^{int} E\pm; E; 0\rangle$
108.1	$\sum_{\Gamma_{ph}, \tilde{q}, \xi} E\pm; E; \Gamma_{ph}, \tilde{q}, \xi\rangle \langle \dots H^{int} E\pm; E; 0\rangle$

TABLE II: Natural basis of subspaces \mathcal{H}_{E+}^* and \mathcal{H}_{E-}^* . The bra $\langle \dots |$ is the adjoint of the preceding ket.

B. Stationary States and Strong Coupling

The problem of finding the stationary dot states, *i.e.* QDPs, consists in the eigenvalue problem

$$H^{QDP} |\Gamma j, m\rangle = \epsilon_{\Gamma, m} |\Gamma j, m\rangle \quad (42)$$

where m is a sequential energy index inside a particular symmetry (Γ, j). This eigenvalue equation was solved individually inside each of the three decoupled subspaces $\mathcal{H}_{A_1}^*$, \mathcal{H}_{E+}^* and \mathcal{H}_{E-}^* using the enhanced matrix diagonalization method outlined in section III D. The three resulting spectra are given in Fig. 7 (red, green, blue). A geometrical representation of the corresponding polaron states is shown in Fig. 8, where the closed surfaces are isosurfaces of the electronic and vibrational probability density functions. Those functions were obtained by computing the respective partial traces,

$$\rho_{lattice}(\mathbf{x}) = \langle \mathbf{x} | Tr_{lattice} (|\Gamma j, m\rangle \langle \Gamma j, m|) | \mathbf{x} \rangle \quad (43)$$

$$\rho_{electron}(\mathbf{x}) = \langle \mathbf{x} | Tr_{electron} (|\Gamma j, m\rangle \langle \Gamma j, m|) | \mathbf{x} \rangle \quad (44)$$

The two-dimensional representation E necessarily exhibits a spectrum consisting of twice degenerate levels, each of which is associated with one state in \mathcal{H}_{E+}^* and one state in \mathcal{H}_{E-}^* . Each superposition $c_+ |E+, m\rangle + c_- |E-, m\rangle$ is again a stationary state.

Both the ground level and the first excited level yield negative energy shifts. This is consistent with the general feature that the ground level of *each representation* is necessarily lowered with respect to corresponding free level. The numerical values of these shifts are $\Delta\epsilon = -2.0$ meV and $\Delta\epsilon = -2.5$ meV. The same

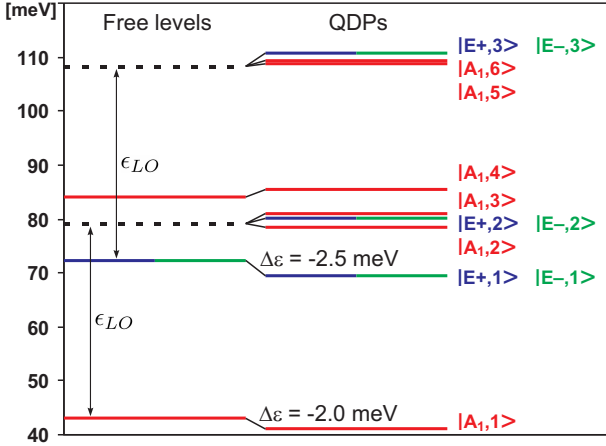


FIG. 7: Spectrum of low energy quantum dot polarons (QDPs). Inside each symmetry subspace the states have been labelled with an energy index m , such that $m = 1$ corresponds to lowest energy state of a given symmetry.

shifts computed with 2nd order perturbation theory are $\Delta\varepsilon = -7.0$ meV and $\Delta\varepsilon = -17.4$ meV, respectively. This manifest large failure of a perturbative approach clearly confirms the existence of a strong coupling inside *both* irreps (A_1 , E).

C. Coupling Substructure

For further characterization of the coupling regime it is interesting to consider the two state sets \mathcal{S}_1 and \mathcal{S}_2 , defined as

$$\begin{aligned} \mathcal{S}_1 &\equiv \{|A_1, 1\rangle, |A_1, 3\rangle, |A_1, 6\rangle\} \\ \mathcal{S}_2 &\equiv \{|A_1, 2\rangle, |A_1, 4\rangle, |A_1, 5\rangle\} \end{aligned} \quad (45)$$

The A_1 -states of Fig. 8 have been ordered according to these sets. We demonstrated numerically that states in \mathcal{S}_1 are to a good approximation contained in the subspace $\mathcal{H}_{A_1,1}^* \subset \mathcal{H}_{A_1}^*$ defined in Tab. I. Indeed, the norms of their projections on $\mathcal{H}_{A_1,1}^*$ exceed 95% of the full norms. With the same accuracy the states in \mathcal{S}_2 are contained in $\mathcal{H}_{A_1,2}^* \subset \mathcal{H}_{A_1}^*$. In other words, the two subspaces $\mathcal{H}_{A_1,1}^*$ and $\mathcal{H}_{A_1,2}^*$ appear *reasonably decoupled*, although the whole subspace $\mathcal{H}_{A_1}^* \equiv \mathcal{H}_{A_1,1}^* \oplus \mathcal{H}_{A_1,2}^*$ constitutes a strong coupling regime. Therefore the strong coupling regime must reside inside the two subspaces $\mathcal{H}_{A_1,1}^*$ and $\mathcal{H}_{A_1,2}^*$ individually, and they may be referred to as "weakly coupled strong coupling subspaces". The physical reason for this particular structure relies in the geometry of the vibrational density function $\rho_{lattice}(\mathbf{x})$. Fig. 8 shows that states in \mathcal{S}_1 have a vibrational component, which is vertically centered in the dot, whereas the states in \mathcal{S}_2 have *two* centers of vibration splitting the isosurface in two parts. Indeed the subspace $\mathcal{H}_{A_1,1}^*$ is spanned by two one-phonon states with vertically centered vibrational density and one zero-phonon state with centered

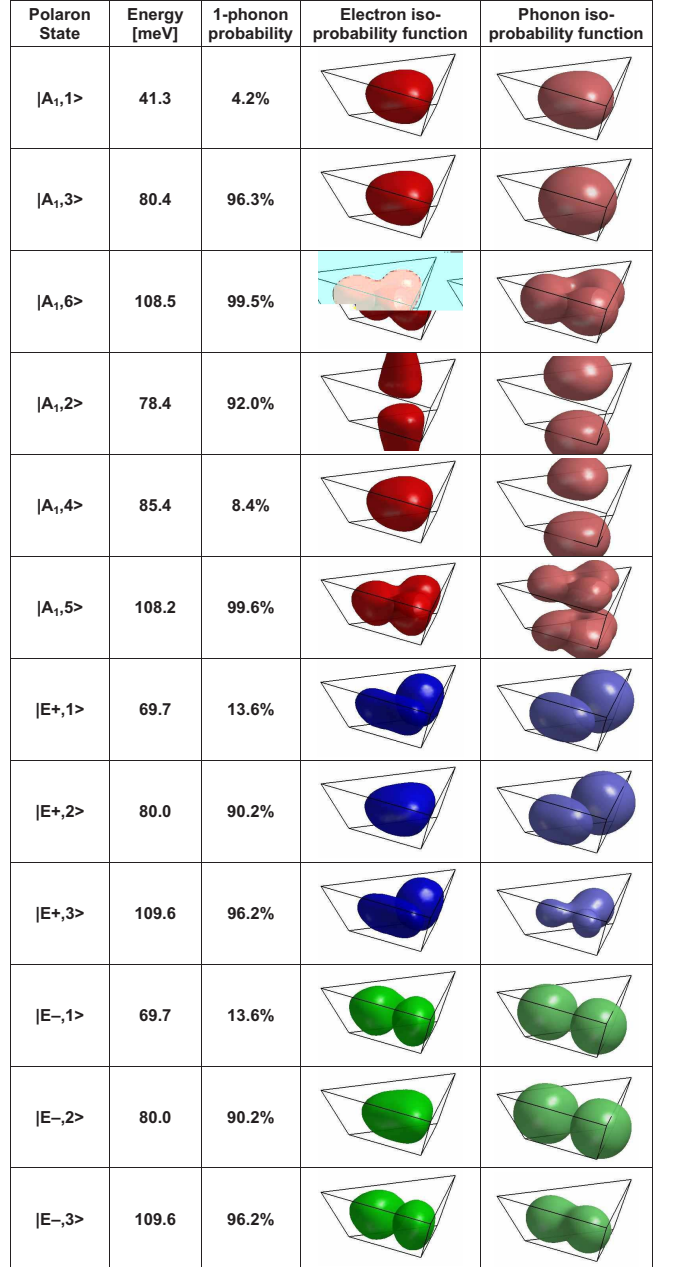


FIG. 8: Geometrical representation of QDPs. The two right columns show isosurfaces of the electronic and vibrational probability density functions in direct space.

electronic density. The resulting overlap leads to a strong interaction between electrons and phonons. The same conclusion applies to the subspace $\mathcal{H}_{A_1,2}^*$, where the density functions are vertically split in two parts. One the other hand, this picture reveals that the mutual overlap between $\mathcal{H}_{A_1,1}^*$ and $\mathcal{H}_{A_1,2}^*$ is considerably smaller.

The concept of weakly coupled subspaces $\mathcal{H}_{A_1,1}^*$ and $\mathcal{H}_{A_1,2}^*$ provides a direct tool for interpretation of the spectrum in Fig. 7. In particular, the ground levels of each subspace, *i.e.* $|A_1, 1\rangle$ and $|A_1, 2\rangle$, are necessarily lowered relative to the corresponding free levels. Analogically, the most excited levels of each subspaces, *i.e.* $|A_1, 5\rangle$ and

$|A_1, 6\rangle$, are both raised. Their mutual splitting remains very small as they are to a good approximation uncoupled.

Finally, we emphasize that the novel concept of "weakly coupled strong coupling subspaces" $\mathcal{H}_{\Gamma j,1}^*, \mathcal{H}_{\Gamma j,2}^*, \dots$ is very general and to a certain extent applicable to all QDs. If the matrix element integral is close to zero due to the mutual orthogonality of the electronic wave functions, these subspaces can be treated as decoupled in a good approximation. This idea is straightforward when working with the natural basis, and thus represents a further advantage of using non-orthogonal basis states.

D. Entanglement measure and strong coupling, decoherence and relaxation

An alternative characterization of the strong coupling is reflected in the entanglement of stationary dot states, *i.e.* QDPs. We have computed the entanglement between electronic and phononic coordinates using the standard measure introduced by Bennett *et al.*²⁸ For pure states,

$$Ent(|\Gamma j, m\rangle) \equiv \sum_{i=1}^N |c_i|^2 \log_N |c_i|^2 \quad (46)$$

where the coefficients c_i are given by the diagonal Schmidt decomposition

$$|\Gamma j, m\rangle = \sum_{i=1}^N c_i |e_i\rangle \otimes |ph_i\rangle \quad (47)$$

It is known that this form always exists for every particular ket $|\Gamma j, m\rangle$, but the computation of the $|\Gamma j, m\rangle$ -dependent orthogonal vectors $\{|e_i\rangle\}$ and $\{|ph_i\rangle\}$, in the electronic and phononic Hilbert spaces respectively, *now requires a preliminary orthogonalisation of the quantum dot phonon basis $B_{\mu\mu'}^\dagger |0\rangle$* which can be elegantly performed via a Choleski decomposition of the Λ matrix. A subsequent singular value decomposition (SVD) of the coefficient matrix in the tensorial product basis will deliver c_i . It is remarkable that the sum over i in (47) can be limited to the number of electron states N because of the properties of the SVD. The entanglement measure (46) can vary between 0 (non-entangled) and 1 (fully entangled), and is also often equivalently called the "entropy of mixing" of the two subsystems in state $|\Gamma j, m\rangle$.

Tab. III shows the entanglement of the QDPs presented in Fig. 8. Weakly entangled states ($Ent \lesssim 0.1$) can be considered as an electron enwrapped by a localized phonon. In the present case, such a picture applies to the two QDPs $|A_1, 1\rangle$ and $|A_1, 3\rangle$. Numerically, they consist to 99.5% of two natural basis states, which *both* involve the *same* electronic state $|A_1, 1\rangle$ (first two basis states in Tab. I). Hence, the QDPs $|A_1, 1\rangle$ and $|A_1, 3\rangle$ can be considered as the electron state $|A_1, 1\rangle$, enwrapped with different orthogonal phonons. All other QDPs are

strongly entangled ($Ent \gtrsim 0.1$) with no adequate perturbative picture. Particularly strong entanglement is found in the states $|A_1, 5\rangle$ and $|A_1, 6\rangle$, which involve peculiar Bell-state superpositions inside the E -representation of the form $|E+\rangle \otimes |E+\rangle + |E-\rangle \otimes |E-\rangle$. This of course suggests a general tendency to find particularly strongly entangled polarons in dots with symmetry related degeneracies.

State	Entanglement	Phonon Number	Relax. Factor
$ A_1, 1\rangle$	0.023	0.042	0.001
$ A_1, 3\rangle$	0.007	0.963	0.007
$ A_1, 6\rangle$	0.523	0.995	0.520
$ A_1, 2\rangle$	0.203	0.920	0.186
$ A_1, 4\rangle$	0.222	0.084	0.019
$ A_1, 5\rangle$	0.517	0.996	0.515
$ E\pm, 1\rangle$	0.256	0.136	0.035
$ E\pm, 2\rangle$	0.245	0.902	0.221
$ E\pm, 3\rangle$	0.229	0.962	0.220

TABLE III: Entanglement, 1-phonon probability and heuristic "relaxativity measure" of the Quantum Dot Polarons (QDPs) in the pyramidal dot with $h = 10mn$.

Finally, we should nevertheless discuss a further possible connection between entanglement and phonon-mediated decoherence and relaxation. A simple model of such decoherence and relaxation would additionally account for a weak bulk interaction between "quantum dot phonons" and "pseudo phonons" or "quantum dot phonons" and LA-phonons. In a perturbative approach, this typically results in a finite lifetime for QDPs, which would otherwise be everlasting. One may expect that the decoherence time indeed depends on the entanglement between electronic and phononic coordinates, since entanglement manifests strong quantum correlations that would also be sensitive to phonon-phonon interactions and effectively induce electron state hopping. Nevertheless it also depends on the weight of the phonon component. Hence, we may heuristically propose a "relaxativity measure" for QDPs, defined as the product of the entanglement and the average phonon number

$$Rel(|\Gamma j, m\rangle) \equiv \langle \Gamma j, m | \sum_{\lambda\lambda'} (\Lambda_{\lambda\lambda'}^{-1} B_\lambda^\dagger B_{\lambda'} | \Gamma j, m \rangle \times Ent(|\Gamma j, m\rangle) \quad (48)$$

In the present one-phonon model this measure varies between 0 (everlasting) and 1 (short coherence time, say $\sim 1ps$). At thermal equilibrium the dot state is represented by a density matrix exhibiting a high probability of states with a low relaxativity measure and vice versa. This measure does not really measure the relaxation since relaxation also implies other factors like resonances and population of final states, this is why we speak of "relaxativity". It has the status of a rough heuristic guess, since it is not the result of a proper relaxation model describing realistically phonon-phonon interactions and

in particular neglects any dependence on the particular geometry.

E. Dot size variation

We shall now discuss the variation of the polaron spectrum as a function of a varying dot height h . Figure 9 shows the varying spectrum of H^0 (free levels) and the spectrum of H^{QDP} (quantum dot polarons) in the restricted energy band [40 meV, 120 meV] (quadratically extrapolated from explicit computations of the dot heights 10 nm, 7.5 nm and 5 nm). To gain clarity and to remain consistent with the disappearance of certain free levels for smaller dots, we have restricted the graph to the two lowest levels of the two subspaces $\mathcal{H}_{A_1,1}^*$ and \mathcal{H}_{E+}^* . The latter is of course degenerate with \mathcal{H}_{E-}^* and the respective levels are twice degenerate.

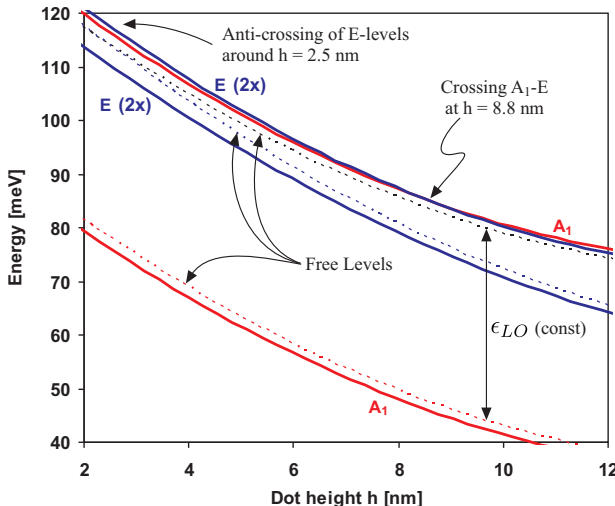


FIG. 9: Spectrum in function of the dot height h . (dashed lines) free electronic energies obtained by diagonalizing H^0 , (solid lines) polaron energies obtained by diagonalizing H^{QDP} .

There are three relevant free energies, the electronic ground level with symmetry A_1 (red dashed line), the first excited level with symmetry E (blue dashed line), and the electronic ground level combined with one phonon (black dashed line). The latter two undergo a crossing in the vicinity of the dot height $h = 2.5\text{ nm}$. By virtue of the resulting resonance, the two E -like polaron levels (blue solid lines) exhibit maximal energy shifts around $h = 2.5\text{ nm}$ ($\Delta\epsilon \approx 5\text{ meV}$) giving rise to a level anti-crossing. On the other hand, the decreasing resonance for increasing dot height, leads to a true crossing between the first excited E -like polaron level (upper blue solid line) and the first excited A_1 -like polaron level (upper red solid line). Such a true crossing is consistent with the strict analytical decoupling stemming from group theoretical arguments (*i.e.* different irreps).

V. INSIGHTS ON LOW ENERGY SCHEME IN QDS

We shall now expand the results to a very general class of QDs, including pyramidal, spherical, cubic or even cylindrical ones. For all these systems we uncover an analogous low energy spectrum, clear connections between polarons and free levels, symmetry properties and qualitative dot size dependencies.

Explicitly, we consider all dots with a non-degenerate electronic ground level and a twice degenerate first electronic excitation. These dots include the special but predominant class of dots with C_{nv} symmetry with $n \geq 3$. Qualitatively, they yield a low-energy polaron spectrum consisting of two shifted electron levels and a splitted electron+phonon level, see Fig. 10. Group theory reveals three independent substructures (red, blue, green), where two are mutually degenerate (blue, green). This structure can be deduced analytically from the natural basis (36), or may be obtained from the spectrum studied above (Fig. 7) by suppressing all QDPs with higher energies or associated with the third electron level.

The relative position of the first excited polaron in the invariant representation (here $|A_1, 3\rangle$) depends on whether the free electronic energy spacing is larger or smaller than the constant phonon energy ϵ_{LO} , see Fig. 7a and Fig. 7b. In case (a), the state $|A_1, 3\rangle$ can fall between the second electron level (blue/green) and the electron+phonon level (dashed level). In (b), the same state always lies above the free electron+phonon level. This feature is a straightforward consequence of the connections between free levels and dot polarons (fine dashed lines) resulting from the natural basis (36).

For a given dot, one can generally pass from situation (a) to (b) by a dot size increase rendering the electronic energy spacing smaller than ϵ_{LO} . The varying spacing between the upper two free levels leads to a changing shift of the two degenerate QDP levels (blue/green). This changes are represented by the vertical arrows for increasing dot size. The dependence gets reversed when passing from case (a) to (b), due to the anti-crossing at the resonance. The shift of the two symmetrical polaron levels (red) is dot size independent, because of their symmetry-decoupling from other levels and the constant phonon energy ϵ_{LO} .

The fine dashed lines in Fig. 10 give proper and general connections between the free electronic levels and QDP levels, and allow to interpret the variation of level shifts with size. Although they reflect our own specific coupling schemes, described with group theory, they have a generic nature and are typically applicable in the general case of C_{nv} -like symmetry (with $n \geq 3$). For example they are in agreement with the findings of Verzelen *et al.*¹⁹ for the perfectly analogous case of cylindrical dots (height/radius=12/18). Case (a) is obtained for radii $< 13\text{ nm}$, whilst case (b) correspond to radii $> 13\text{ nm}$. Following the discussion above, it is straightforward to understands that in their case $|1\pm\rangle$ lies below $|S1\rangle$, that $|2\pm\rangle$ lies above $|P\pm0\rangle$ and that $|\tilde{S}1\rangle$ can only lie below

$|P \pm 0\rangle$ for radius < 13 nm. We also see that the shifts of $|\tilde{S}0\rangle$ and $|\tilde{S}1\rangle$ do not depend on the dot size due to symmetry decoupling and the constant spacing between $|S0\rangle$ and $|S1\rangle$.

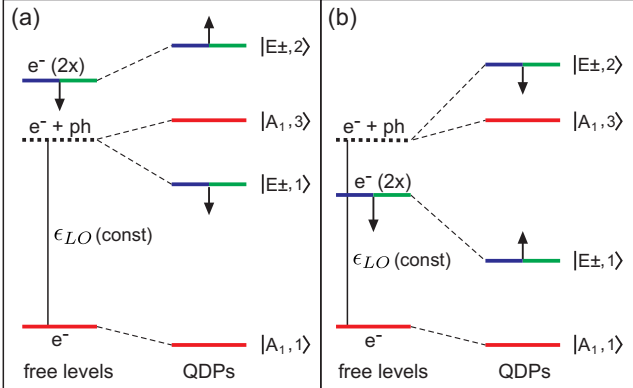


FIG. 10: Fundamental level structure for QDs with C_{nv} -like symmetry with $n \geq 3$. (a) electronic energy spacing exceeds phonon energy ϵ_{LO} , typically smaller dots. (b) electronic energy spacing smaller than ϵ_{LO} , typically larger dots. The arrows show the directions of level shifts with increasing dot size.

VI. SUMMARY

In this work we uncovered the substantial advantage of the direct use of non-orthogonal creation and annihilation operators to address the strong electron-phonon coupling in QDs. Starting from a general viewpoint, we fully reformulated the polaron problem in terms of those operators that naturally appear in the interaction Hamiltonian and generate the phonons relevant for individual transitions between electronic eigenstates. For the first time, we also provided a complementary basis for all non-coupling phonons, which play a sensitive role in relaxation processes mediated by phonon-phonon interactions. Even though one might a priori be skeptic with the use of non-orthogonal objects, this approach proved mathematically elegant and fruitful for physical insights. In particular, we found that the coupling structure between electrons and phonons follows a tree-like structure in Hilbert space, which allowed us to find a non-trivial rule to truncate the Hilbert space in the case of a finite phonon number. This striking feature was consistently applied to a general QD structure in a one-electron/one-phonon model leading to a novel and reduced basis for polarons, herein baptized the "natural basis". The latter marks an efficient tool for computation and detailed classification of quantum dot polarons (QDPs) linked with one-phonon excitations. Beyond the case of general quantum dots, we also investigated degenerate and symmetrical quantum dots using the appropriate mathematical instruments, namely group theory. This reveals additional simplifications, degeneracies and subclasses of QDPs.

As a realistic application we computed in 3D the low-

energy QDPs of recently manufactured pyramidal QDs with C_{3v} -symmetry. To this end an efficient adaptive irregular discretization of the lattice mode space was developed to compute the Fröhlich matrix elements, and the generalized eigenvalue problem stemming from the direct use of non-orthogonal basis vectors was directly fed into efficient matrix diagonalization software. In this way we were able to remarkably decrease the required computational resources. The numerical results explicitly revealed the spectral structure predicted from the natural basis. 3D-visualizations of the stationary polaronic dot states gave insight in the localization of both electronic and phononic components and showed the different symmetry properties. Dot size dependent spectral investigations uncovered level crossings and anti-crossings, which were consistent with the corresponding symmetry properties. Further, we could prove the existence of strong coupling regimes for each symmetry representation through explicit comparison with second order perturbation theory. Yet, there was undoubtable numerical evidence for the presence of very weakly coupled subspaces within the strong coupling regimes. This led us to the novel concept of "weakly coupled strong coupling subspaces". Using the natural basis such weakly coupled strong coupling subspaces could be understood in terms of specifically different overlaps between electronic wave functions and non-orthogonal vibrational modes. To characterize the coupling between electronic and phononic coordinates in the QDP eigenstates we discussed for the first time the use of Bennett's entanglement measure and we proposed a possible heuristic "relaxativity measure". Finally, the low-energy spectrum of a fundamental class of QDs (including spherical, cubic and cylindrical dots) was discussed using the symmetrized natural basis, and we could provide precise qualitative predictions on the level structure and dot size dependance, as much for the general case and for our specific case of C_{3v} pyramidal QDs.

VII. APPENDIX

A. Phonon Operator Transformations

We shall give explicit expressions for the phonon operator transformation (5) and (7) referred in section II B. The first law of transformation (5), i.e. $\{b_{\mathbf{q}}^\dagger\} \rightarrow \{B_\lambda^\dagger\}$, was given in definition (3),

$$B_\lambda^\dagger \equiv \sum_{\mathbf{q}} L_{\lambda\mathbf{q}}^* b_{\mathbf{q}}^\dagger \quad (49)$$

$$\Rightarrow \Lambda_{\lambda\lambda'} \equiv [B_\lambda, B_{\lambda'}^\dagger] = \sum_{\mathbf{q}} L_{\lambda'\mathbf{q}}^* L_{\lambda\mathbf{q}} \quad (50)$$

To find the remaining relations, i.e. $\{b_{\mathbf{q}}^\dagger\} \rightarrow \{B_{\mathbf{q}}^\dagger\}$ and $\{b_{\mathbf{q}}^\dagger\} \leftarrow \{B_\lambda^\dagger, B_{\lambda'}^\dagger\}$, we use the definition (4), i.e. $B_{\mathbf{q}}^\dagger \equiv (\mathbf{1} - \mathcal{P}) b_{\mathbf{q}}^\dagger$, where \mathcal{P} is the orthogonal projector \mathcal{P} on the phonon subspace generated by $\{B_\lambda^\dagger\}$. In particular, this

definition implies

$$B_{\mathbf{q}}^{\dagger}|0\rangle = (\mathbf{1} - \mathcal{P}') b_{\mathbf{q}}^{\dagger}|0\rangle \quad (51)$$

where $|0\rangle$ is the phonon vacuum and \mathcal{P}' is the restriction of \mathcal{P} to the one-phonon subspace, satisfying

$$\mathcal{P}' B_{\lambda}^{\dagger}|0\rangle = B_{\lambda}^{\dagger}|0\rangle \quad (52)$$

Like any operator acting exclusively in the subspace $\text{vect}\{B_{\lambda}^{\dagger}|0\rangle\}$, \mathcal{P}' can be expressed as

$$\mathcal{P}' = \sum_{\lambda\lambda'} p_{\lambda\lambda'} B_{\lambda}^{\dagger}|0\rangle\langle 0|B_{\lambda'} \quad (53)$$

with complex coefficients $p_{\lambda\lambda'}$. Substituting (53) in (52) and using the commutation relations (50) yields the unique solution $p_{\lambda\lambda'} = (\Lambda)_{\lambda\lambda'}^{-1}$. Hence,

$$\begin{aligned} \mathcal{P}' &= \sum_{\lambda\lambda'} (\Lambda)_{\lambda\lambda'}^{-1} B_{\lambda}^{\dagger}|0\rangle\langle 0|B_{\lambda'} \\ &= \sum_{\mathbf{q}\mathbf{q}'} \sum_{\lambda\lambda'} (\Lambda)_{\lambda\lambda'}^{-1} L_{\lambda\mathbf{q}}^* L_{\lambda'\mathbf{q}'}^* b_{\mathbf{q}}^{\dagger}|0\rangle\langle 0|b_{\mathbf{q}'} \end{aligned} \quad (54)$$

Substituting this expression in (51) yields the second transformation law $\{b_{\mathbf{q}}^{\dagger}\} \rightarrow \{B_{\mathbf{q}}^{\dagger}\}$,

$$B_{\mathbf{q}}^{\dagger} = \sum_{\mathbf{q}'} c_{\mathbf{q}\mathbf{q}'} b_{\mathbf{q}'}^{\dagger} \quad (55)$$

with

$$c_{\mathbf{q}\mathbf{q}'} = \delta_{\mathbf{q}\mathbf{q}'} - \sum_{\lambda\lambda'} (\Lambda)_{\lambda\lambda'}^{-1} L_{\lambda\mathbf{q}}^* L_{\lambda'\mathbf{q}'} \quad (56)$$

Combined with definition (49) this gives the third transformation law $\{b_{\mathbf{q}}^{\dagger}\} \leftarrow \{B_{\lambda}^{\dagger}, B_{\mathbf{q}}^{\dagger}\}$,

$$b_{\mathbf{q}}^{\dagger} = B_{\mathbf{q}}^{\dagger} + \sum_{\lambda\lambda'} L_{\lambda'\mathbf{q}} (\Lambda^{-1})_{\lambda\lambda'} B_{\lambda}^{\dagger} \quad (57)$$

which concludes the transformation $\{b_{\mathbf{q}}\} \leftrightarrow \{B_{\lambda}, B_{\mathbf{q}}\}$.

Using these expressions it is possible to derive the fundamental commutators

$$[b_{\mathbf{q}}, B_{\mathbf{q}'}^{\dagger}] = c_{\mathbf{q}'\mathbf{q}} \quad (58)$$

$$[B_{\mathbf{q}}, B_{\mathbf{q}'}^{\dagger}] = \sum_{\mathbf{q}''} c_{\mathbf{q}\mathbf{q}''}^* c_{\mathbf{q}'\mathbf{q}''} \quad (59)$$

$$[B_{\lambda}, B_{\mathbf{q}}^{\dagger}] = 0$$

the last one is given as eq. (6) in the main text.

Finally, the expression of the phonon number operator (7) of section II B is deduced using relation (57). It is helpful to derive first the relations of linear dependence between the overcomplete set of operators $B_{\mathbf{q}}^{\dagger}$,

$$\sum_{\mathbf{q}} L_{\lambda\mathbf{q}}^* B_{\mathbf{q}}^{\dagger} = 0 \quad \forall \lambda \quad (60)$$

Using these relations, eq. (57) readily implies eq. (7) of the main text.

B. Derivation of the coupling structure

Step 1: Proof of relation (21) for $m = 0$.

$$\begin{aligned} &D^+ \mathcal{H}_{k\text{ph}}^{QSP} \\ &\equiv \bigoplus_{\mu} \text{vect} \left\{ \sum_{\mu'} \left[a_{\mu}^{\dagger} a_{\mu'} |\mu_0\rangle \otimes B_{\mu\mu'}^{\dagger} B_{\mu'_1\mu_1}^{\dagger} \cdots B_{\mu'_k\mu_k}^{\dagger} |0\rangle \right] \right\} \\ &= \text{vect} \left\{ |\mu\rangle \otimes B_{\mu\mu_0}^{\dagger} B_{\mu'_1\mu_1}^{\dagger} \cdots B_{\mu'_k\mu_k}^{\dagger} |0\rangle; \forall \mu, \mu_i, \mu'_i \right\} \\ &\equiv \mathcal{H}_{k+1\text{ph}}^{QSP,1} \end{aligned} \quad (61)$$

Step 2: Proof of relation (21) for $m > 0$.

By recurrence, similar to step 1.

Step 3: Proof of relation (22).

First note that relation (20) implies

$$D^- \mathcal{H}_{k\text{ph}}^{QSP,0} \supset D^- \mathcal{H}_{k\text{ph}}^{QSP,1} \supset D^- \mathcal{H}_{k\text{ph}}^{QSP,2} \quad (62)$$

On the other hand, the image via the operator D^- must necessarily be a subspace of \mathcal{H}^{QSP} , and hence

$$D^- \mathcal{H}_{k\text{ph}}^{QSP,0} \subset \mathcal{H}_{k-1\text{ph}}^{QSP} \quad (63)$$

Thus, in order to prove (22) for $m = 0, 1, 2$, it is necessary and sufficient to show this relation for $m = 2$, i.e.

$$D^- \mathcal{H}_{k\text{ph}}^{QSP,2} = \mathcal{H}_{k-1\text{ph}}^{QSP} \quad (64)$$

To this end let us construct a chain of subspaces $\mathcal{S}_1 \subset \mathcal{S}_2 \subset \dots \subset \mathcal{S}_{k-1}$ of

$$\begin{aligned} &D^- \mathcal{H}_{k\text{ph}}^{QSP,2} \\ &\equiv \text{vect} \left\{ |\nu_1\rangle \otimes B_{\nu_1\nu_2} B_{\nu_2\nu_3}^{\dagger} B_{\nu_3\mu_1}^{\dagger} B_{\mu'_2\mu_2}^{\dagger} \cdots B_{\mu'_{k-2}\mu_{k-2}}^{\dagger} |0\rangle \right\} \end{aligned} \quad (65)$$

The first subspace $\mathcal{S}_1 \subset D^- \mathcal{H}_{k\text{ph}}^{QSP,2}$ is obtained by choosing $\mu_i = \nu_2$ and $\mu'_i = \nu_3$, $\forall i = 1, \dots, k-2$,

$$\mathcal{S}_1 \equiv \text{vect} \left\{ |\nu_1\rangle \otimes B_{\nu_1\nu_2} B_{\nu_2\nu_3}^{\dagger} (B_{\nu_3\nu_2}^{\dagger})^{k-1} |0\rangle \right\} \quad (66)$$

For real electronic wave functions (a choice, which is always possible), we have $B_{\nu_3\nu_2}^{\dagger} = B_{\nu_2\nu_3}^{\dagger}$. Using this relation and the generally non-vanishing commutator $[B_{\nu_1\nu_2}, B_{\nu_2\nu_3}^{\dagger}] = \Lambda_{(\nu_1\nu_2)(\nu_2\nu_3)}$, gives

$$\mathcal{S}_1 = \text{vect} \left\{ |\nu_1\rangle \otimes (B_{\nu_2\nu_3}^{\dagger})^{k-1} |0\rangle \right\} \quad (67)$$

A second particular subspace $\mathcal{S}_2 \subset D^- \mathcal{H}_{k\text{ph}}^{QSP,2}$ can be defined by choosing $\mu_i = \nu_2$ and $\mu'_i = \nu_3$, but only for $i = 1, \dots, k-3$.

$$\begin{aligned} \mathcal{S}_2 &= \text{vect} \left\{ |\nu_1\rangle \otimes B_{\nu_1\nu_2} (B_{\nu_2\nu_3}^{\dagger})^{k-1} B_{\mu'_1\mu_1}^{\dagger} |0\rangle \right\} \\ &= \text{vect} \left\{ |\nu_1\rangle \otimes (\alpha (B_{\nu_2\nu_3}^{\dagger})^{k-1} + \beta (B_{\nu_2\nu_3}^{\dagger})^{k-2} B_{\mu'_1\mu_1}^{\dagger}) |0\rangle \right\} \end{aligned} \quad (68)$$

where we have relabeled $(k-2) \rightarrow 1$. There is a relationship between α and β resulting from the commutators. Yet, by adding to each vector a particular vector of $\mathcal{S}_1 \subset \mathcal{S}_2$ on can get rid of the terms scaling in α and obtain

$$\mathcal{S}_2 \equiv \text{vect} \left\{ |\nu_1\rangle \otimes (B_{\nu_2\nu_3}^{\dagger})^{k-2} B_{\mu'_1\mu_1}^{\dagger} |0\rangle \right\} \quad (69)$$

A third particular subspace $\mathcal{S}_3 \subset D^- \mathcal{H}_{k ph}^{QSP,2}$ is obtained by choosing $\mu'_i = \nu_2$ and $\mu_i = \nu_3$ for $i = 1, \dots, k-4$,

$$\begin{aligned} \mathcal{S}_3 &= \text{vect} \left\{ |\nu_1\rangle \otimes B_{\nu_1 \nu_2} (B_{\nu_2 \nu_3}^\dagger)^{k-2} B_{\mu'_1 \mu_1}^\dagger B_{\mu'_2 \mu_2}^\dagger |0\rangle \right\} \\ &= \text{vect} \left\{ |\nu_1\rangle \otimes (\alpha (B_{\nu_2 \nu_3}^\dagger)^{k-2} B_{\mu'_1 \mu_1}^\dagger + \beta (B_{\nu_2 \nu_3}^\dagger)^{k-2} B_{\mu'_2 \mu_2}^\dagger + \gamma (B_{\nu_2 \nu_3}^\dagger)^{k-3} B_{\mu'_1 \mu_1}^\dagger B_{\mu'_2 \mu_2}^\dagger) |0\rangle \right\} \end{aligned} \quad (70)$$

By adding to each vector a particular vector of $\mathcal{S}_2 \subset \mathcal{S}_3$, we can get rid of the terms scaling in α and β . Thus,

$$\mathcal{S}_3 \equiv \text{vect} \left\{ |\nu_1\rangle \otimes (B_{\nu_2 \nu_3}^\dagger)^{k-3} B_{\mu'_1 \mu_1}^\dagger B_{\mu'_2 \mu_2}^\dagger |0\rangle \right\} \quad (71)$$

This method can be repeated to successively generate the spaces

$$\mathcal{S}_j \equiv \text{vect} \left\{ |\nu_1\rangle \otimes (B_{\nu_2 \nu_3}^\dagger)^{k-j} B_{\mu'_1 \mu_1}^\dagger \cdots B_{\mu'_{j-1} \mu_{j-1}}^\dagger |0\rangle \right\} \quad (72)$$

up to $j = k-1$, where no condition is imposed on the indices μ'_i and μ_i . This last space writes

$$\begin{aligned} \mathcal{S}_{k-1} &= \text{vect} \left\{ |\nu_1\rangle \otimes B_{\nu_2 \nu_3}^\dagger B_{\mu'_1 \mu_1}^\dagger \cdots B_{\mu'_{k-2} \mu_{k-2}}^\dagger |0\rangle \right\} \\ &= \text{vect} \left\{ |\nu_1\rangle \otimes B_{\mu'_1 \mu_1}^\dagger \cdots B_{\mu'_{k-1} \mu_{k-1}}^\dagger |0\rangle \right\} \\ &\equiv \mathcal{H}_{k-1 ph}^{QSP} \end{aligned} \quad (73)$$

Therefore,

$$\mathcal{H}_{k-1 ph}^{QSP} \subset D^- \mathcal{H}_{k ph}^{QSP,2} \quad (74)$$

On the other hand, tie image via the operator D^- must necessarily be a subspace of \mathcal{H}^{QSP} , and hence

$$\mathcal{H}_{k-1 ph}^{QSP} \supset D^- \mathcal{H}_{k ph}^{QSP,2} \quad (75)$$

It follows that

$$\mathcal{H}_{k-1 ph}^{QSP} = D^- \mathcal{H}_{k ph}^{QSP,2} \quad (76)$$

which is sufficient and necessary for relation (22), as explained above.

C. Expression of H^{int} for an irregular q-space discretization

In the Fröhlich matrix elements (2), the quantization volume V (direct space) dictates the underlying q-space discretization, such that each \mathbf{q} occupies a volume of $\Omega = (2\pi)^3/V$. This can be seen by taking V as a cubic volume with periodic boundary conditions, for which the Fröhlich interactions was originally derived. If we use an *irregular* space discretization with varying cell sizes $\Omega(\mathbf{q})$, the constant quantization volume V must consequently be replaced by a function,

$$V \rightarrow V(\mathbf{q}) = \frac{8\pi^3}{\Omega(\mathbf{q})} \quad (77)$$

In the present case, $\Omega(\mathbf{q})$ was taken as the Wigner-Seitz volume around the point \mathbf{q} in a given irregular reciprocal space discretization.

D. C_{3v} -Symmetrized Phonon Basis

We consider the symmetrized one-phonon states

$$|\Gamma, j, \vec{q}\rangle \equiv \alpha \mathcal{P}_{(\Gamma, j)} |\vec{q}\rangle = \sum_{g \in C_{3v}} c_{\Gamma j}(g) |\mathcal{R}(g)\vec{q}\rangle \quad (78)$$

where $\mathcal{R}(g)$ is the symmetry operation associated with the group element g and $\mathcal{P}_{\Gamma, j}$ is the projector on the subspace associated with the irrep Γ and the partner function j . α is a normalization factor defined up to a phase factor by the normalization relations

$$\langle \Gamma, j, \vec{q} | \Gamma, j, \vec{q} \rangle = 1 \quad \forall \Gamma, j, \vec{q} \quad (79)$$

By projecting the n_{modes} basis states $|\vec{q}\rangle$ on the four subspaces associated with A_1 , A_2 , $E+$ and $E-$, one obtains an overcomplete set of $4n_{modes}$ states, which necessarily obeys $3n_{modes}$ relations of linear dependence. Those relations can be identified with the symmetry transformation relations,

$$A_1 : |A_1, \mathcal{R}(g)\vec{q}\rangle = |A_1, \vec{q}\rangle \quad \forall g \in C_{3v} \quad (80)$$

$$A_2 : |A_2, \mathcal{R}(g)\vec{q}\rangle = \begin{cases} +|A_2, \vec{q}\rangle & g = I, C_3^+, C_3^- \\ -|A_2, \vec{q}\rangle & g = \sigma_1, \sigma_2, \sigma_3 \end{cases} \quad (81)$$

$$E : \begin{cases} |E\pm, \mathcal{R}(\sigma_1)\vec{q}\rangle = \pm |E\pm, \vec{q}\rangle \\ |E\pm, \vec{q}\rangle + |E\pm, \mathcal{R}(C_3^+)\vec{q}\rangle + |E\pm, \mathcal{R}(C_3^-)\vec{q}\rangle = 0 \end{cases} \quad (82)$$

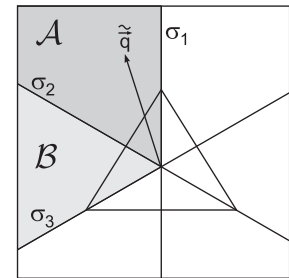


FIG. 11: Partition of the set of available wave vectors \mathbf{q} . The whole set can be obtained by applying symmetry operations of the C_{3v} group on the subset \mathcal{A} .

For the irrep A_1 the five non-trivial relations of (80) for a given \vec{q} allow to restrict the plane wave set $\{\vec{q}\}$ to the sixth marked \mathcal{A} in Fig. 11. The set $\{|A_1, \tilde{\vec{q}}\rangle, \tilde{\vec{q}} \in \mathcal{A}\}$ is orthonormal. An analog reasoning applies to the irrep A_2 based on the five non-trivial relations of (81). For the irrep E , (82) yields two non-trivial relations for a given vector \vec{q} and a given partner function $j = \pm$. Hence the set $\{\vec{q}\}$ may be restricted to a third of its elements, represented by $\mathcal{A} \cup \mathcal{B}$ in Fig. 11. Any two states $|E, j, \tilde{\vec{q}}\rangle$ and $|E, j, \mathcal{R}(\sigma_2)\tilde{\vec{q}}\rangle$ with $\tilde{\vec{q}} \in \mathcal{A}$ (and hence $\mathcal{R}(\sigma_2)\tilde{\vec{q}} \in \mathcal{B}$) are non-orthogonal. In order to achieve orthogonality

and to use *one fixed vector set for all irreps*, we introduce the states

$$\begin{aligned} |E\pm, \tilde{q}, \xi=1\rangle &\equiv |E\pm, \tilde{q}\rangle \mp |E\pm, \sigma_2 \tilde{q}\rangle \quad (83) \\ |E\pm, \tilde{q}, \xi=2\rangle &\equiv |E\pm, \tilde{q}\rangle \pm |E\pm, \sigma_2 \tilde{q}\rangle \end{aligned}$$

where $\tilde{q} \in \mathcal{A}$ and hence $\mathcal{R}(\sigma_2)\tilde{q} \in \mathcal{B}$. This definition completes the construction of the one phonon part of the phonon basis (40). The new index $\xi = 1, 2$ permits the restriction of plane wave vectors to the sixth \mathcal{A} and has the following physical interpretation: All E -states with $\xi = 1$ involve *one* plane wave amplitude, whereas the E -states with $\xi = 2$ mix *two* different amplitudes (see Fig. 6c).

The canonical transformation relating the symmetrized one-phonon basis to the plane wave basis $\{|\tilde{q}\rangle\}$ results from the definitions (78) and (83) and the normalization relation (79). We find,

$$\begin{pmatrix} |A_1, \tilde{q}\rangle \\ |A_2, \tilde{q}\rangle \\ |E, +, \tilde{q}, 1\rangle \\ |E, +, \tilde{q}, 2\rangle \\ |E, -, \tilde{q}, 1\rangle \\ |E, -, \tilde{q}, 2\rangle \end{pmatrix} = U \begin{pmatrix} |\tilde{q}\rangle \\ |\mathcal{R}(\sigma_2)\tilde{q}\rangle \\ |\mathcal{R}(C_3^+)\tilde{q}\rangle \\ |\mathcal{R}(\sigma_3)\tilde{q}\rangle \\ |\mathcal{R}(C_3^-)\tilde{q}\rangle \\ |\mathcal{R}(\sigma_1)\tilde{q}\rangle \end{pmatrix} \quad \forall \tilde{q} \in \mathcal{A} \quad (84)$$

with the unitary transformation matrix

$$U = \begin{pmatrix} \frac{1}{\sqrt{6}} & \frac{1}{\sqrt{6}} & \frac{1}{\sqrt{6}} & \frac{1}{\sqrt{6}} & \frac{1}{\sqrt{6}} & \frac{1}{\sqrt{6}} \\ \frac{1}{\sqrt{6}} & -\frac{1}{\sqrt{6}} & \frac{1}{\sqrt{6}} & -\frac{1}{\sqrt{6}} & \frac{1}{\sqrt{6}} & -\frac{1}{\sqrt{6}} \\ \frac{1}{2} & -\frac{1}{2} & 0 & 0 & -\frac{1}{2} & \frac{1}{2} \\ \frac{1}{\sqrt{12}} & \frac{1}{\sqrt{12}} & -\frac{1}{\sqrt{3}} & -\frac{1}{\sqrt{3}} & \frac{1}{\sqrt{12}} & \frac{1}{\sqrt{12}} \\ \frac{1}{2} & \frac{1}{2} & 0 & 0 & -\frac{1}{2} & -\frac{1}{2} \\ \frac{1}{\sqrt{12}} & -\frac{1}{\sqrt{12}} & -\frac{1}{\sqrt{3}} & \frac{1}{\sqrt{3}} & \frac{1}{\sqrt{12}} & -\frac{1}{\sqrt{12}} \end{pmatrix} \quad (85)$$

E. C_{3v} -Symmetrized Tensor Product Basis

Based on the symmetrized electron basis (39) and the symmetrized phonon basis (40), we shall construct symmetrized product states. The zero-phonon state $|0\rangle$ belonging to the irrep A_1 , the symmetrized product states involving zero phonons readily write,

$$\begin{aligned} |A_1; A_1, \alpha_e; 0\rangle &\equiv |A_1, \alpha_e\rangle \otimes |0\rangle \quad (86) \\ |E\pm; E; 0\rangle &\equiv |E\pm\rangle \otimes |0\rangle \end{aligned}$$

where $n = 1, 2$ is the electronic energy index inside A_1 . Semicolons separate intrinsic polaron, electron and phonon indices. As for the symmetrized product states involving one phonon, one uses Clebsh-Gordon coeffi-

cients,

$$\begin{aligned} |A_1; A_1, \alpha_e; A_1, \tilde{q}\rangle &\equiv |A_1, \alpha_e\rangle \otimes |A_1, \tilde{q}\rangle \\ |A_1; E; E, \tilde{q}, \xi\rangle &\equiv \frac{1}{\sqrt{2}} \left(|E+\rangle \otimes |E+, \tilde{q}, \xi\rangle \right. \\ &\quad \left. + |E-\rangle \otimes |E-, \tilde{q}, \xi\rangle \right) \\ |A_2; A_1, \alpha_e; A_2, \tilde{q}\rangle &\equiv |A_1, \alpha_e\rangle \otimes |A_2, \tilde{q}\rangle \\ |A_2; E; E, \tilde{q}, \xi\rangle &\equiv \frac{1}{\sqrt{2}} \left(|E+\rangle \otimes |E-, \tilde{q}, \xi\rangle \right. \\ &\quad \left. - |E-\rangle \otimes |E+, \tilde{q}, \xi\rangle \right) \\ |E\pm; A_1, \alpha_e; E, \tilde{q}, \xi\rangle &\equiv |A_1, \alpha_e\rangle \otimes |E\pm, \tilde{q}, \xi\rangle \\ |E\pm; E; A_1, \tilde{q}\rangle &\equiv |E\pm\rangle \otimes |A_1, \tilde{q}\rangle \\ |E\pm; E; A_2, \tilde{q}\rangle &\equiv |E\mp\rangle \otimes |A_2, \tilde{q}\rangle \\ |E\pm; E; E, \tilde{q}, \xi\rangle &\equiv \frac{1}{\sqrt{2}} \left(|E+\rangle \otimes |E\pm, \tilde{q}, \xi\rangle \right. \\ &\quad \left. \mp |E-\rangle \otimes |E\mp, \tilde{q}, \xi\rangle \right) \end{aligned}$$

where $\xi = 1, 2$ is the additional phonon index used for E -like one-phonon states.

¹ D. L. Huffaker, G. Park, Z. Zou, O. B. Shchekin, and D. G. Deppe, *Appl. Phys. Lett.* **73**, 2564 (1998).

² S.-W. Lee, K. Hirakawa, and Y. Shimada, *Appl. Phys. Lett.* **75**, 1428 (1999).

³ Ch. Santori, M. Pelton, G. Solomon, Y. Dale, and Y. Yamamoto, *Phys. Rev. Lett.* **86**, 1502 (2001).

⁴ M. Pelton, Ch. Santori, J. Vuckovic, B. Zhang, G. Solomon, J. Plant, and Y. Yamamoto, *Phys. Rev. Lett.* **89**, 233602 (2002).

⁵ M. Han, X. Gao, J. Z. Su, and S. Nie, *Nature Biotechnology* **19**, 631 (2001).

⁶ X. Wu, H. Liu, J. Liu, K. Haley, J. Treadway, J. Larson, N. Ge, F. Peale, and M. Bruchez, *Nature Biotechnology* **21**, 41 (2003).

⁷ R. D. Schaller and V. I. Klimov, *Phys. Rev. Lett.* **92**, 186601 (2004).

⁸ F. Klopff, R. Krebs, J. P. Reithmaier, and A. Forchel, *IEEE Photon. Technol. Lett.* **13**, 764 (2001).

⁹ D. Loss and D. P. DiVincenzo, *Phys. Rev. A* **57**, 120 (1998).

¹⁰ U. Bockelmann and G. Bastard, *Phys. Rev. B* **42**, 8947 (1990).

¹¹ H. Benisty, C. M. Sotomayor-Torres, and C. Weisbuch, *Phys. Rev. B* **44**, 10945 (1991).

¹² K. Brunner, U. Bockelmann, G. Abstreiter, M. Walther, G. Böhm, G. Tränkle, and G. Weimann, *Phys. Rev. Lett.* **69**, 3216 (1992).

¹³ U. Bockelmann, *Phys. Rev. B* **48**, 17637 (1993).

¹⁴ M. Notomi, M. Naganuma, T. Nishida, T. Tamamura, H. Iwamura, S. Nojima, and M. Okamoto, *Appl. Phys. Lett.* **58**, 720 (1991).

¹⁵ S. Raymond, S. Fafard, S. Charbonneau, R. Leon, D. Leonard, P. M. Petroff, and J. L. Merz, *Phys. Rev. B* **52**, 17238 (1995).

¹⁶ T. Inoshita and H. Sakaki, *Phys. Rev. B* **56**, R4355 (1997).

¹⁷ K. Kral and Z. Khas, *Phys. Status Solidi B* **208**, R5 (1998).

¹⁸ S. Hameau, Y. Guldner, O. Verzelen, R. Ferreira, G. Bastard, J. Zeman, A. Lemaître, and J.M. Gerard *Phys. Rev. Lett.* **83**, 4152 (1999).

¹⁹ O. Verzelen, R. Ferreira, and G. Bastard, *Phys. Rev. B* **62**, R4809 (2000).

²⁰ T. Stauber, R. Zimmermann, and H. Castella, *Phys. Rev. B* **62**, 7336 (2000).

²¹ T. Stauber and R. Zimmermann, *Phys. Rev. B* **73**, 115303 (2006).

²² R. Ferreira, O. Verzelen, and G. Bastard, *Phys. Status Solidi B* **238**, 575 (2003).

²³ D. Gammon, E.S. Snow, B.V. Shanabrook, D.S. Katzer, D. Park, *Phys. Rev. Lett.* **76**, 3005 (1996).

²⁴ P. Tronc, V.P. Smirnov, K.S. Zhuravlev, *Phys. Status Solidi B* **241**, 2938 (2004).

²⁵ E. Kapon, E. Pelucchi, S. Watanabe, A. Malko, M. H. Baier, K. Leifer, B. Dwir, F. Michelini, and M.-A. Dupertuis, *Physica E* **25**, 288 (2004).

²⁶ H. Fröhlich, H. Pelzer, and S. Zienau, *Philos. Mag.* **41**, 221 (1950).

²⁷ F. Michelini, M.-A. Dupertuis, and E. Kapon, *Appl. Phys. Lett.* **84**, 4086 (2004).

²⁸ C. H. Bennett, H. J. Bernstein, S. Popescu, B. Schumacher, *Phys. Rev. A* **53**, 2046 (1996).